

**Mathematical Modelling of Glioma Stem Cell
Fractions After Irradiation
Treatments**

By
Wafa Veljee

A thesis submitted in partial fulfillment of the requirements for the degree of

MASTER OF SCIENCE

In

APPLIED MATHEMATICS

DEPARTMENT OF MATHEMATICAL AND STATISTICAL SCIENCES

UNIVERSITY OF ALBERTA

©Wafa Veljee, 2014

Abstract

Glioblastoma Multiforme (GBM) is a grade IV brain tumour. It is the most common brain malignancy and is extremely aggressive. Ionizing radiation plays a vital role in the treatment of this tumour. Growth of the GBM is sustained by a subpopulation of the tumour cells often called the glioma stem cells (GSC). Kim *et al.* and Gao *et al.* presented *in vitro* and *in silico* data respectively where GSC population seemed unnaturally increased. We created four nested ODE models for GBM growth. Parameters were estimated from the available data using the least squares error method and the Akaike Information Criterion was used to choose a suitable model for tumour growth. The aspect of irradiation treatment was incorporated into the glioma growth model using the linear-quadratic model. My analysis on the treatment ODE model supports the findings of Gao *et al.* that the increased stem cell ratios can only be explained if the stem cell population divides more aggressively after radiotherapy.

Acknowledgements

I wish to express my deep gratitude to my academic advisor and my M.Sc thesis supervisor, professor Thomas Hillen. Dr. Hillen has been extremely generous with his time, knowledge and support in the two years that I spent at the University of Alberta.

I am grateful to my examining committee for their careful consideration of my thesis. Dr. de Vries and Dr. Wang, along with Dr. Hillen, provided valuable insight on my research project.

I would have not been able to enjoy this research experience if it had not been for the friends I made at University of Alberta's Centre for Mathematical Biology. I received constant guidance from my office-mate and superior, Dr. Diana White, and my academic siblings, Amanda Swan and Andreas Buttenschoen. I applaud my friends, Carlos Contreras, Jody Reimer, Philippe Gaudreau and Valerie Budd, for not only picking me up when I needed it but also pushing me forward. Last, but certainly not the least, I thank my family.

The people mentioned above made my transition into Canadian life effortless and also very lovely.

Contents

Abstract	ii
Acknowledgements	iii
Contents	iv
List of Figures	vi
List of Tables	viii
Abbreviations	ix
1 Introduction	1
1.1 Glioblastoma Multiforme: why must we study it?	1
1.2 Outline of the thesis	3
1.3 Comparing healthy versus glioma stem cells	4
1.4 Mathematical modelling and relevant literature	7
1.4.1 “Acute and fractionated irradiation differentially modulate glioma stem cell division kinetics” X. Gao, T. McDonald, L. Hlatky and H.Enderling.	8
1.4.2 “The tumour growth paradox and immune system-mediated selection for cancer stem cells” T. Hillen, H. Enderling and P. Hahnfeldt.	17
2 Modelling glioma growth using Ordinary Differential Equations	24
2.1 A model with stem and non-stem cells	24
2.1.1 Fixed points and stability analysis	26
2.2 Models with quiescence	29
3 Data fitting and model comparison	32
3.1 Estimating parameters to fit data	32
3.1.1 The least-squares error method	33
3.1.2 Data fit using the optimal parameter set	34
3.1.3 Improving the data fit	34
3.2 Model comparison using the Akaike Information Criterion	37
3.3 Conclusion	38
4 Mathematics of the derivation of radiation treatment: The Linear-Quadratic Model	39
4.1 The Linear-Quadratic Model	39

4.2	Hazard Function	42
5	Glioma stem cell model with radiation treatment	45
5.1	ODE results and comparison with experimental data	46
5.2	Cell behaviour changes after irradiation treatment	49
6	Sensitivity analysis	50
6.1	Main results	53
7	Discussion	55
7.1	Future work: Adding quiescence to our model using a delay	55
7.2	Discussion and Conclusions	57

List of Figures

1.1	MRI scans of GBM demonstrate the fast growth of this tumour.	2
1.2	Theories of GBM genesis.	6
1.3	Magnification of the CPM lattice.	8
1.4	Lattice update in the CPM.	10
1.5	CPM simulation for tumour growth.	12
1.6	<i>In vitro</i> GSC% calculated 48 hours after the last irradiation dose.	13
1.7	GSC% calculated 48 hours after the last irradiation dose using the CPM.	15
1.8	GSC numbers calculated for all treatment styles using the CPM.	16
1.9	Total cell numbers calculated for all treatment styles using the CPM.	16
2.1	Symmetric and asymmetric division in glioma stem cells.	25
2.2	Compartmental figure for model U,V.	25
2.3	Phase portrait highlighting biologically significant invariant region.	28
2.4	Phase portrait containing numerous numerical solution trajectories.	29
2.5	Compartmental figure for model U,V,Qu.	30
2.6	Compartmental figure for model U,V,Qv.	30
2.7	Compartmental figure for model U,V,Qu,Qv.	30
3.1	Data fitting for Model U,V: no quiescence.	35
3.2	Data fitting for Model U,V,Qu: quiescence attributed to stem cells (U) only.	35
3.3	Data fitting for Model U,V,Qv: quiescence attributed to cancer cells (V) only.	36
3.4	Data fitting for Model U,V,Qu,Qv: quiescence attributed to both stem cells (U) and cancer cells (V).	36
4.1	Lethal DNA damage due to ionizing radiation.	40
4.2	The hazard function for a single ionizing radiation treatment.	44
4.3	The hazard function for fractionated ionizing radiation treatment.	44
5.1	Numerical ODE solutions for tumour growth and treatment.	47
5.2	Bar graph comparing GSC% determined experimentally with those calculated by the ODE model.	49
6.1	Sensitivity of GSC% on the parameters p_s and k_G for single dose treatment.	52
6.2	Sensitivity of GSC% on the parameters p_s and k_G for fractionated dose treatment.	52
6.3	Bar graph comparing GSC% determined experimentally with those calculated by the modified ODE model.	54

7.1	Bar graph comparing GSC% calculated by the CPM and differential equation models that contain the property of quiescence with those that do not contain this assumption.	57
7.2	Bar graph comparing GSC% determined experimentally with those calculated by the ODE and DDE models.	57

List of Tables

3.1	Comparing models using the Akaike Information Criterion.	37
4.1	Experimentally determined values of the radio-sensitivity and radio-protection coefficients.	42
7.1	Values of parameters used throughout the thesis.	60

Abbreviations

CPM	C ellular P otts M odel
GBM	G lio B lastoma M ultiforme
GSC	G lioma S tem C ells
IR	I onizing R adiation
NSC	N eural S tem C ells
TIC	T umour I nitiating C ells

Chapter 1

Introduction

1.1 Glioblastoma Multiforme: why must we study it?

Glioblastoma Multiforme (GBM) is a grade IV brain tumour. It is the most common and an extremely aggressive brain malignancy [15, 17, 20, 25, 26]. According to the World Health Organization, the median survival period after treatment is 14.6 months (just over a year!) [25]. There are 17,000 new patients diagnosed with GBM every year in the USA alone [18].

GBM has a high growth rate and the rapid division of glioma cells requires oxygen. In addition to that, this tumour has poor vasculature. Therefore, hypoxia (deprivation of oxygen) is a common feature in GBM tumours. Other characteristics of GBM are existence of necrotic regions and blood vessels that are irregular and chaotic [20].

Metastasis is rare in GBM tumours [26]. This may be because the short survival time of GBM patients is not enough for frequent metastasis. In fact, after treatment, most tumours will reoccur at the primary site where the tumour was originally found. This is because GBM tumour's cells are extremely penetrative and disperse deep into the brain tissue, hence, complete removal by surgery is nearly impossible. This phenomenon is demonstrated in Figure 1.1.

Treatment mainly includes ionizing radiation with surgery. However, the diffuse tissue distribution often makes the surgical removal of GBM difficult or ineffective [15, 25]. In addition to that, this tumour's cells are known to acquire resistance to cytotoxic

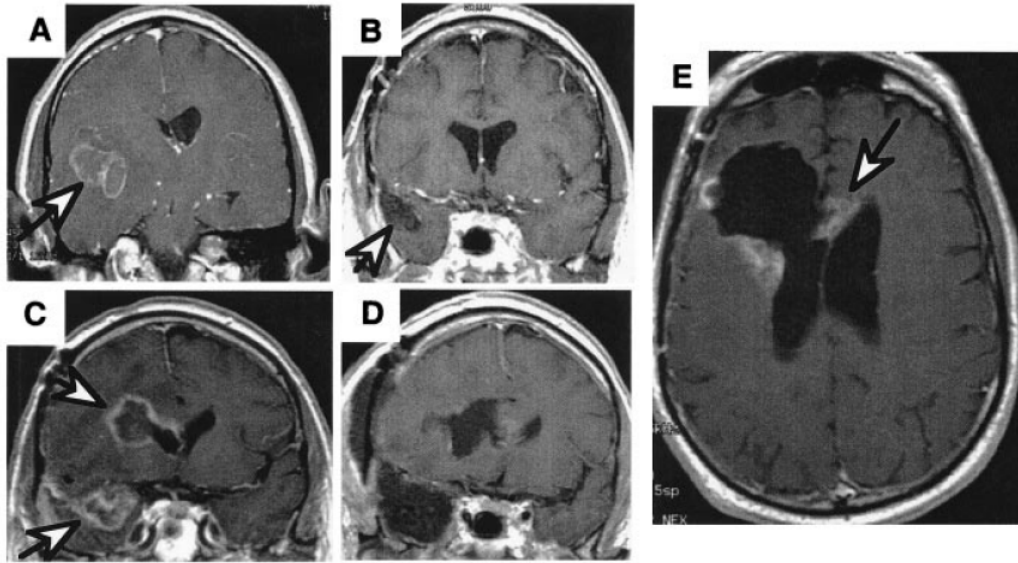


FIGURE 1.1: This figure demonstrates the fast growth rate of GBM tumours and how ineffective surgical resection can be. These are MRI scans from a patient with GBM before and after treatment [15]. (A) The arrow points to the pre-surgical tumour. (B) The arrow points to the clear cavity after surgical removal. (C) The arrows point to the surgical margins where tumour returns, 6 months after the surgery. (D) Removal of the secondary tumours is conducted with surgery. (E) Tumour returns at resection margin within 3 months and has spread into the neighbouring hemisphere.

treatment [27]. Therefore, ionizing radiation plays a vital role in the treatment procedure of this tumour. Even though numerous studies have been conducted over the past decades and there have been great advances in therapy, the survival rates of the patients have not improved [17]. Therefore, it is essential that the dynamics of GBM tumours be studied.

GBM comprises of a heterogenous set of mutated cells that are extremely infiltrative. It has been discovered recently that the growth of the GBM is sustained by a subpopulation of tumour cells called the glioma stem cells (GSC). These cells are also known to acquire resistance to chemotherapy. These cells not only have tumour-initiating but also high-proliferation powers. The glioma stem cells make the glioblastoma multiforme an extensively invasive tumour. In Section 1.3 we will talk about glioma stem cells and how they differ from healthy neural stem cells.

1.2 Outline of the thesis

In Sections 1.1 and 1.3 we discussed the biological background of the glioblastoma multiforme tumour. In addition to that, in Section 1.4, we will look at literature that use individual-based and mathematical models to analyze glioma growth. In the following chapters, Chapters 3 and 5, we will analyze data published by Kim et al. [16] and Gao et al. [11]. The experimental data of GBM growth, as published in [16], show an enrichment of GSC in a treated tumour. Gao et al. [11] explained this enrichment via an individual based Cellular Potts Model (CPM).

The goal of my research is to explain the unusual enrichment of stem cells in the *in vitro* tumours [16] using an ordinary differential equation (ODE) model for glioma growth and treatment. In this research we will try to answer the following question: how does ionizing radiation treatment of the GBM tumour encourage the stem cell population to grow more aggressively?

Gao *et al.*'s CPM already looks at the behaviour of GSC after radiotherapy. The CPM provided some valuable insight as to how cell dynamics may change as a result of radiation. We adapted the assumptions of the CPM to create an ODE model. There are many benefits of using an ODE system to model glioma growth. In addition gaining new observations on radiation-induced cell kinetics, our ODE model also allows us to perform mathematical analysis. Compared to the CPM, numerical solutions to ODE systems are calculated efficiently and are computationally inexpensive. In addition to that, a realistic range of parameters for the ODE system is easily estimated from biological studies as these parameters have bio-physical interpretations. These parameters can then be varied over their biologically significant ranges to choose for ones that fit best to data (the least-squares error method is a popular technique to predict parameters). Choosing parameters for the CPM, however, is not as straight forward.

A chapter by chapter breakdown of this project is as follows. In Chapter 2, we construct a differential equation model for the GBM tumour growth and we perform quantitative analysis for the basic model. We will also create models that take detailed assumptions into account. In Chapter 3, we will compute numerical solutions and conduct data fitting, parameter estimation (using the least-squares error method) and test to see which model (basic or the detailed) is the best representation for tumour growth (using

the Akaike Information Criterion). In Chapter 4, we look at the mathematics behind tumour treatment. The concept of “cell death due to treatment” is incorporated into our model in Chapter 5, numerical solutions are calculated and the ODE results are compared with experimental data. In Chapter 6, we will conduct a sensitivity analysis on several parameters to see how the tumour growth is affected by certain parameters, especially after a tumour is exposed to radiotherapy. In Chapter 7, we discuss our findings. For our future work, a delay differential equation model is proposed where the phenomenon of growth arrest is added to our differential equation model.

The main results are that our ODE model for radiotherapy treatment of glioma growth confirms Gao et al.’s results [11] in suggesting that the increment of GSC ratio in an *in vitro* tumour treated with irradiation cannot be explained simply by the resistance of GSC to irradiation. In fact, the cell dynamics of the GSC have to change after radiation treatment. These radiation-induced changes in cell division dynamics include either stem cells dividing into daughter stem cells (symmetric division) rather than differentiating into other types of tumour cells (asymmetric division) or that the stem cell is dividing faster. The dominant mechanism for the increase in GSC fraction in the ODE-simulated GBM is the shorter cell cycle induced by radiotherapy. The increase in the probability of symmetric division alone is not enough to explain the enrichment of GSC ratios in the GBM tumour. The available experimental data [16] considers two treatment scenarios, a single fraction treatment and a multiple fraction treatment. While Gao et al.’s individual based model [11] can only explain data for fractionated treatment, our ODE model fits both treatment scenarios.

1.3 Comparing healthy versus glioma stem cells

Neural stem cells

Recent discovery of continued adult neurogenesis (production of neurons in the brain) implies that there are stem cells present in the brain [25]. Healthy neural stem cells in the central nervous system are essential for normal brain activity. Neural stem cells reside in confined regions in the central nervous system and make up a very small population of the brain cells [17].

Neural stem cells are mitotically active and can differentiate into several types of cells including neurons, astrocytes (glial cells that provide nourishment to neurons and remove waste) and oligodendrocytes (glial cells that support the axon and produce the Myelin sheath), and therefore are responsible for generating most of the differentiated components of the brain [17]. Other properties of these stem cells include extensive proliferation capacity and the ability to maintain and renew their population in the adult human brain.

Glioma stem cells

GBM tumours usually occur in older adults. Hence, this tumour is not inherited or developmental. Instead, genetically unstable tumour-initiating cells form the seed of GBM tumours [17]. Steindler *et al.* were the first scientists to identify cells in a GBM mass that displayed qualities of neural stem cells [25]. These qualities included self-renewal and high multipotency (ability to differentiate into many different kinds of cells). These cells, called the glioma stem cells, also express some of the markers that are specific to healthy stem cells. Additionally, the glioma stem cells possess the properties of repopulation and infinite proliferation capacity. When injected into organisms such as mice (*in vivo*), these cells created new tumours that were invasive and migratory.

Vescovi *et al.* in their review, "*brain tumour stem cells*" discuss the definition of brain tumour stem cells [25]. A cell found in a brain tumour can be classified as a brain tumour stem cell if:

- they initiate tumours when grafted in brain tissue,
- they are capable of regenerating their population,
- they are genetically mutated,
- their differentiation process is faulty, and
- they are able to create non-tumour cells.

Figure 1.2 discusses various theories on how GBM is created [17]. Originally, it was believed that healthy glial cells would mutate to become tumour cells and would divide and form a GBM mass. But recently it has been discovered that neural stem cells, neural

or glial progenitor cells, and even mature glial cells may give rise to tumour-initiating cells that further proliferate into colonies of glioma stem cells.

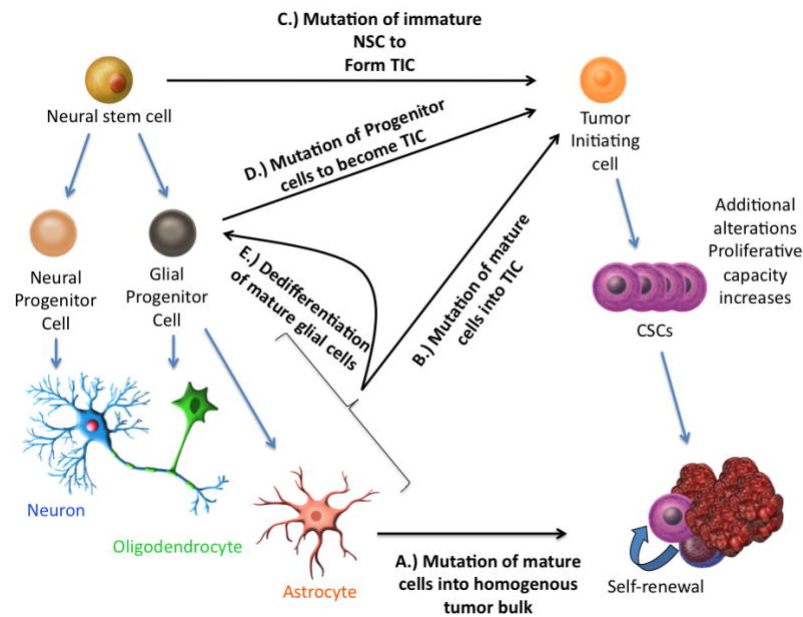


FIGURE 1.2: This figure [17] discusses the theories for GBM genesis. (A) it was thought that mature glial cells mutated and replicated to form tumour masses. But recently evidence suggests that neural stem cells mutate to form tumour initiating cells (TIC) (C), or glial stem cells mutate and become TIC (D), or that differentiated glial cells mutate and become TIC (B). Some literature suggests that differentiated glial cells may dedifferentiate into glial stem cells that mutate and become TIC (E). The TIC then reproduce and form a colony of Glioma stem cells that give rise to a GBM tumour mass.

It is difficult to differentiate between glioma stem cells and the rest of the cells that make up the tumour. Some studies use the CD133 transmembrane protein as a marker for neural and glioma stem cells [17].

Glioma stem cell's ability to renew and repopulate the tumour is dangerous because it means that during treatment if most of the glioma stem cells are not killed or removed, the tumour will return. In fact, even more surprising is that when GBM is irradiated, the glioma stem cells become more aggressive and proliferate with greater fervour. Hence, after the treatment, the growth rate of the tumour becomes larger than if it had received little or no treatment [16].

1.4 Mathematical modelling and relevant literature

Several mathematical and individual-based models exist that discuss the role of tumour stem cells in tumour progression. Ganguli and Puri (2006) [10] and Sole et al. (2008) [22] modelled the evolution of healthy stem cells into cancer stem cells. In 2006, Dingli and Michor [7] used a mathematical model to show that the cancer stem cells drove tumour development. They concluded that “successful therapy must eradicate cancer stem cells”. In 2009, Enderling et al. [9] compared how different cell kinetics parameters impacted tumour growth. In 2012, Hillen and Enderling [14] used differential equations to model the tumour growth paradox (this concept will be described in detail in Section 1.4.2). There has been much work done in this field using individual-based models also. Enderling et al. [8] investigated how cancer stem cells and tumour cells compete for space. Gao et al. [11] constructed a Cellular Potts Model (CPM) to analyze how treatment affects cell division kinetics in the GBM tumour.

We will now discuss the literature that forms the basis of the current project in more detail. These papers are as follows:

1. *Acute and fractionated irradiation differentially modulate glioma stem cell division kinetics.* This paper was written by X. Gao, T. McDonald, L. Hlatky and H. Enderling [11], and discusses an individual-based, Cellular Potts Model for glioma growth.
2. *The tumour growth paradox and immune system-mediated selection for cancer stem cells.* This paper was written by T. Hillen, H. Enderling and P. Hahnfeldt [14]. In this paper a differential equation model for glioma growth is discussed.

We will use the technique of paper 2 to create an ODE model that predicts how the glioma stem cell number changes due to irradiation treatment. We will validate our results using the findings of paper 1.

1.4.1 “Acute and fractionated irradiation differentially modulate glioma stem cell division kinetics” X. Gao, T. McDonald, L. Hlatky and H. Enderling.

Gao et al. used a Cellular Potts Model (CPM) to show how the cell division kinetics of a tumour that undergoes fractionated radiation treatment vary from that of a tumour that undergoes irradiation in a single dose.

The tumour that is being discussed in this study is the GBM tumour that we are already familiar with. The GBM is treated by Ionizing Radiation (IR) with or without surgical removal. Even with treatment, GBM’s prognostic risk is very high. Data from *in vitro* experiments [16] as shown in Figure 1.6, using the U87-MG human GBM line, was used to compare to CPM results.

Mechanism behind the Cellular Potts Model (CPM)

Gao and his fellow researchers [11] used a two-dimensional Cellular Potts Model to simulate GBM growth. This was done by creating a grid that consists of sets of lattice sites that correspond to biological cells (refer to Figure 1.3). This CPM simulation consists of a list of cells, their types, a description of cellular interaction and appropriate initial conditions.

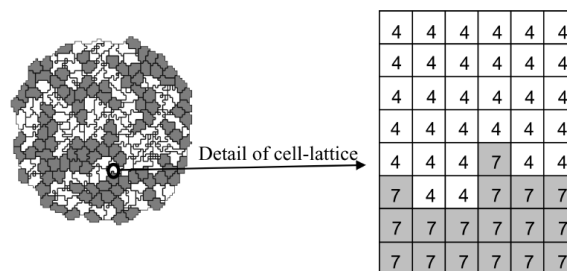


FIGURE 1.3: Magnification of the lattice [23]. Each cell is represented by an index σ , for example, 4 or 7 in this figure. Different types of cells are represented by different colours.

In the Cellular Potts Model (CPM), each lattice point or pixel is denoted by its coordinate vector \vec{i} . Neighbouring lattice sites are represented by \vec{i} and \vec{j} . As shown in Figure 1.3, each cell is a set of pixels. Each cell has a unique index $\sigma(\vec{i})$ (for example, 4 or 7 in Figure 1.3). And the cell type, $\tau(\sigma(\vec{i}))$, is represented by different colours.

The Hamiltonian function, E , calculates cell properties such as the shape of a cell, its movement, its interaction or adhesion with other cells and its response to external signals. These properties will determine how a mass of cell grows. Adhesion is an important biological property. The capability of cells to adhere to one another and to an extracellular matrix is the reason why complex tissue structures exist. In the Cellular Potts Model, this property of adhesion is described by the contact energy term. The contact energy term, $J(\tau(\sigma(\vec{i})), \tau(\sigma(\vec{j})))$, represents the difference in energy due to adhesion between neighbouring cells. This term depends on the cell type, τ , of the neighbouring cells. In addition to the contact energy term, the energy function is restricted by a surface area and a volume constraint term. The parameter $\lambda_{surface}$ is a cell's inverse membrane compressibility and λ_{volume} is its inverse volume compressibility. The surface area and volume constraint energy terms keep the cell close to a target surface area, S_{target} , and a target volume, V_{target} .

$$\begin{aligned}
 E = & \overbrace{\sum_{\vec{i}, \vec{j} \text{ neighbor}} J(\tau(\sigma(\vec{i})), \tau(\sigma(\vec{j}))(1 - \delta(\sigma(\vec{i}), \sigma(\vec{j})))}^{\text{boundary energy term}} \\
 & + \overbrace{\sum_{\sigma(\vec{i})} \lambda_{surface}(\sigma(\vec{i}))(v(\sigma(\vec{i})) - V_{target}(\sigma(\vec{i})))}^{\text{volume constraint energy}} \\
 & + \overbrace{\sum_{\sigma(\vec{i})} \lambda_{surface}(\sigma(\vec{i}))(s(\sigma(\vec{i})) - S_{target}(\sigma(\vec{i})))}^{\text{surface area constraint energy}}.
 \end{aligned}$$

The Kronecker delta function, δ , is non-zero when neighbouring lattice sites belong to the same cell. This means that:

$$\delta(\sigma(\vec{i}), \sigma(\vec{j})) = \begin{cases} 1, & \text{if } \sigma(\vec{i}) = \sigma(\vec{j}), \\ 0, & \text{if } \sigma(\vec{i}) \neq \sigma(\vec{j}). \end{cases}$$

The Cellular Potts Model works by updating cell position and cell growth by using the Hamiltonian function E . Numerous attempts are made in order to copy a lattice site's index to its neighbour. For each attempt, a pixel \vec{i} and a neighbouring pixel \vec{j} are randomly selected. If these pixels belong to the same cell (that is $\sigma(\vec{i}) = \sigma(\vec{j})$)

then no change occurs. If the neighbouring pixels do not belong to the same cell (that is $\sigma(\vec{i}) \neq \sigma(\vec{j})$) then an attempt to copy the pixel \vec{i} 's index onto its neighbour is being made. At each time step, cells try to move into their neighbour's boundary. E is calculated for both, the system with change and the system without change. A negative value of ΔE indicates that this change is favourable. Hence the cell movement will occur. If ΔE is positive, cell movement will occur with a probability of $P = e^{-\Delta E/T}$, where T is the temperature. This process of lattice updates is summarized in Figure 1.4.

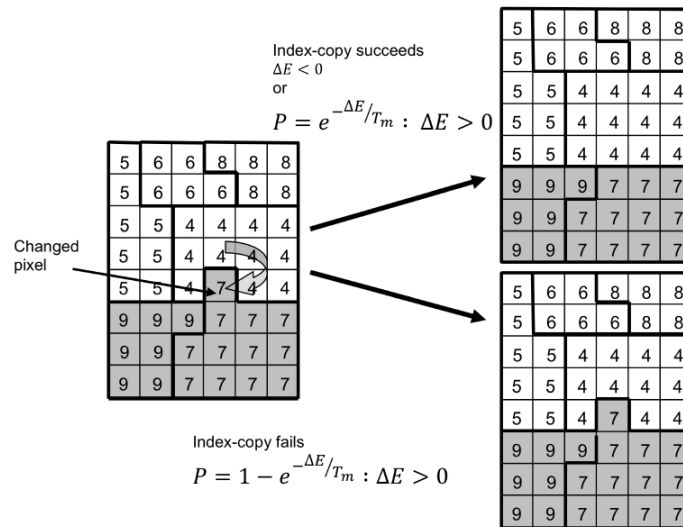


FIGURE 1.4: Conditions for lattice update [23]. The Hamiltonian function is calculated for the event that the cell boundary moves and the event that no movement occurs. The change in Hamiltonians is then calculated. If this value is negative, the lattice is updated and the cell boundary moves. If this value is positive, the cell boundary will move with a probability P .

Modeling GBM growth using CPM

For the Cellular Potts Model, Gao et al. [11] used the following assumptions. The GBM consists of only three kinds of cells. These cells and their properties are listed below:

1. **Glioma Stem Cells (GSC):** these cells have high resistance to IR (ionizing radiation). After an irradiation dose, these cells are able to repair DNA damage and regenerate and hence, are able to repopulate the tumour. These cells are also immortal.
2. **Cancer Cells (CC):** these cells have low resistance to IR and will eventually die.

3. **Quiescent Cells (QC):** these cells have average resistance to IR and are growth-arrested (they neither grow, nor die).

Gao and his team also added the following properties to a CPM so that the area of cells resembled a GBM tumour as much as possible:

- The medium, or the brain, is a 4000 times 4000 pixelated square with periodic boundary conditions.
- Cells grow in area with a growth rate of k until the cell area, $v(\sigma)$ is doubled. The cell then splits into two. This process describes cell division.
- When ΔE is extremely large, that is cell growth is not favourable, the cell becomes growth-arrested (QC).
- GSC may divide symmetrically into two daughter stem cells, with a probability of p_s , or asymmetrically into a daughter stem cell and a daughter cancer cell, with a probability of $1 - p_s$. CC can only divide symmetrically.
- ρ is the proliferation capacity of a cell. A non-zero value of ρ means that a cell is capable of dividing. GSC are immortal having infinite proliferation capacity, so $\rho = \infty$. Whereas the CC have a maximum proliferating capacity, ρ_{max} , of 10 (which means that CC are allowed no more than ten cell divisions). With each CC division, the proliferation capacity decreases.

The result for GBM growth simulation, using the CPM, is shown in Figure 1.5. In this figure a stem cell is placed on the centre of the grid and growth is monitored for 15 days. Snap shots of the CPM grid are taken at day 4, 9 and 15 and compared to pictures from *in vitro* experiments. When compared to experimental tumour growth in petri dishes, the CPM closely predicts the glioma growth found *in vitro*. Hence, the CPM was validated as a good glioma growth model.

Adding irradiation effect to GBM growth model

The CPM for GBM growth results closely resemble *in vitro* tumour growth (refer to Figure 1.5). The next step was to irradiate both, the simulated and the *in vitro*, tumours.

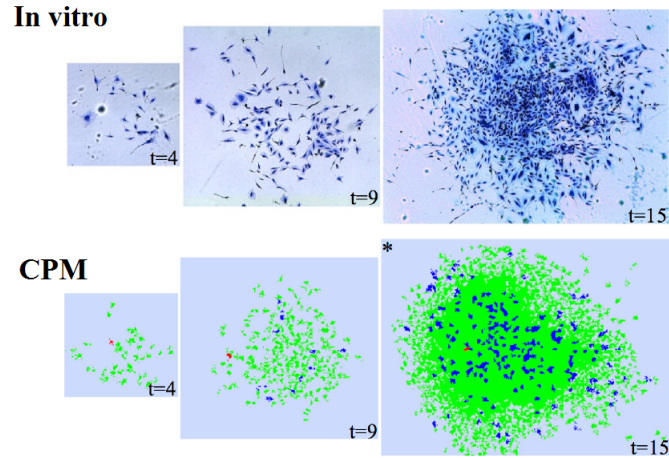


FIGURE 1.5: CPM simulation for tumour growth. The pictures in the top row are from experiments and the snap-shots in the bottom row are from the CPM on day 4, 9 and 15. In the CPM, a GSC is placed in the centre of the grid and growth is monitored for 15 days. Glioma growth in CPM is comparable to the *in vitro* growth of the tumour [11]. In the CPM simulation, the GSC are red, CC are green and the QC are blue.

Adding IR effect to the CPM was done by using the linear-quadratic (LQ) model (more detail about the LQ model is covered in Chapter 4). The following equation calculates the ratio of cells that survive a radiation dose d :

$$S = e^{-\lambda_i(\alpha d + \beta d^2)},$$

where $i = GSC, CC$ and QC . The parameter α measures the radiosensitivity of single-hit killing, β is the radiosensitivity parameter of double-hit killing, λ_i is the radioprotection factor of cell type i .

Gao et al. studied three cases:

1. **Control case:** The tumour received no IR treatment.
2. **Single Treatment:** A single dose of 6 Gy (Gray) was administered.
3. **Fractionated treatment:** Three doses of 2 Gy were administered, each one administered a day apart.

Both the *in vitro* and the CPM tumours were allowed to grow. 48 hours after the last treatment, the percentage of GSC present in these tumours was calculated. The stem cell percentage from Kim *et al.*'s *in vitro* experiments are shown in Figure 1.6 [16]. The authors used the stem cell percentages from the U87 glioma cell line and compared these fractions with those calculated from the CPM. The results are discussed below:

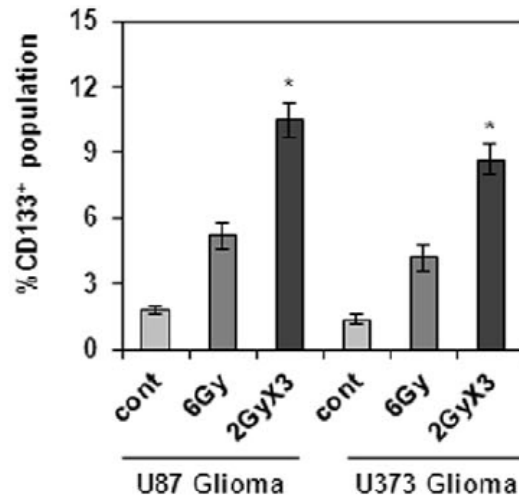


FIGURE 1.6: *In vitro* GSC% calculated 48 hours after the last irradiation dose [16]. The error bars depict the standard deviation from six experiments. The lightest grey bar represents the case where the tumour receives no treatment. The medium grey bar represents the case where the tumour receives 6 Gy units of radiotherapy administered on a single day. And the darkest grey bar represents the case where the GBM tumour receives 2 Gy units of radiation administered on 3 consecutive days. U87 and U373 are glioma cell lines. For comparison with *in silico* results, we will use the GSC percentages from the U87 cell line.

The case 1 (control) results, for both *in vitro* and CPM, matched closely. The percentages of GSC in these tumors are 1.84% and 1.8% respectively. In case 2 (single treatment), a slight overestimation of the GSC% observed *in vitro* by the CPM. Gao concluded that this may be due to the larger portions of CC death in the CPM that were not observed *in vitro*. The greatest discrepancy, however was observed in case 3, the fractionated treatment case. The percentage of GSC in *in vitro* were a lot larger than what the CPM predicted. The fact that GSC have high resistance to IR alone does not explain this discrepancy. Gao and his team researched why the ratios of GSC in *in vitro* tumours that receive fractionated treatment are so high.

The ratio of stem cells in the CPM-simulated tumour is lower than that *in vitro*. To increase the stem cell ratio in the CPM for the fractionated treatment the authors tried the case where stem cells were not allowed to become quiescent after the irradiation. The resultant stem cell percentage is demonstrated by the centre red bar in Figure 1.7 labeled “3x2 Gy: No GSC arrested”. The stem cell percentage did increase as stem cells stayed active even after treatment. However, this increase in stem cell ratios was not significantly higher.

The authors proposed that the enrichment of stem cells *in vitro* was not just a result of

radio-resistance of stem cells. Instead, the stem cell population is aggressively increasing. Gao hypothesized that the division kinetics of GSC change as a result of repeated exposure to radiation. It has been shown that radiation activates the AKT/ cyclin D1/Cdk4 pathway in human glioblastoma cells. Activation of this pathway results in stem cells having a shorter G1 phase and hence, a shorter cell cycle. In addition to this, Gao hypothesized that multiple exposures to irradiation causes a shift from asymmetric to symmetric division.

These hypotheses were adapted to the CPM and are summarized below:

1. An increase in the probability of symmetric division, due to radiation treatment
2. Radiation induces a shorter cell cycle, and
3. Radiation induces a combination of both, the increase in probability of symmetric division and shorter cell cycle.

CPM results using the hypotheses 1, 2 and 3

The bar graph in Figure 1.7 shows that incorporating the three hypotheses in the CPM predict *in vitro* results closely. This paper's main result was that an increase in the symmetric division of the glioma stem cells (from 35% to 75%) or an increase in the speed of cell cycle of the glioma stem cells (from a slow cell cycle of 25 hours to a significantly faster cell cycle of 12 hours) explains the enrichment of glioma stem cells in the tumour after repeated radiotherapy. In fact, the increase in the symmetric division is claimed to be the dominant mechanism for increasing the GSC fraction in the tumour that undergoes fractionated irradiation.

Once the model's stem cell ratios were compared with *in vitro* results, Gao went on to calculate the glioma growth rates, calculated by the CPM, in all three treatment cases: control, single and fractionated irradiation treatment of tumours. Figure 1.8 compares the number of GSC in all CPM simulated cases. It is easy to observe that tumours that receive fractionated treatment contain more GSC than tumours that received a single treatment or no treatment. As GSC are aggressive cells that are able to regenerate and repopulate the tumour, presence of high numbers of GSC in a treated tumour is of concern.

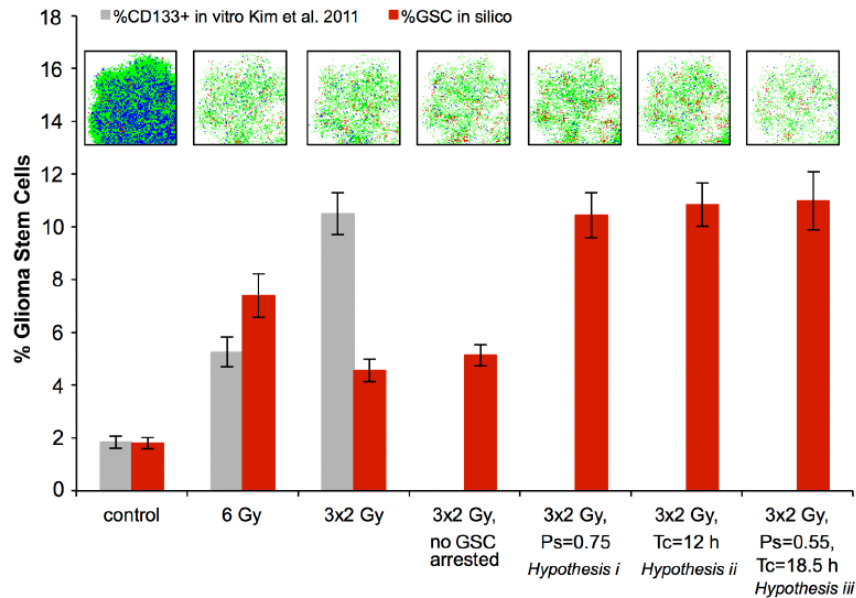


FIGURE 1.7: This bar graph [11] describes the GSC% 2 days after the last treatment dose. The gray bars are GSC% determined *in vitro*. The error bars depict the standard deviation from six experiments. The red bars are GSC% calculated using the CPM. The error bars depict the standard deviation from five simulations. The last three red bars on the right-hand side represent the GSC% calculated using the CPM after applying hypotheses 1, 2 and 3. The three hypotheses closely approximate the GSC% to that of the tumour created with fractionated dose *in vitro*. Two days after the last IR treatment, snapshots were taken of the CPM glioma growth and are shown in the top row in this figure. The GSC are red, CC are green and QC are blue.

Figure 1.9 compares the total number of cells in all simulated cases. In other words, this is a comparison of the mass of the simulated tumours. These findings are astonishing! The CPM predicts that tumours that receive fractionated treatment eventually outgrow the control tumour that receives no treatment. The condition has been observed *in vitro* and is called the tumour growth paradox.

Figures 1.8 and 1.9 describe the other major result of this paper. Fractionated irradiation treatment selects, and hence, increases the population of glioma stem cells. These cells, due to their aggressive and immortal nature, are responsible for the accelerated regrowth of the tumour. So tumours that are exposed to radiation multiple times can have higher growth rates and worse prognoses than tumours that are treated once or not at all.

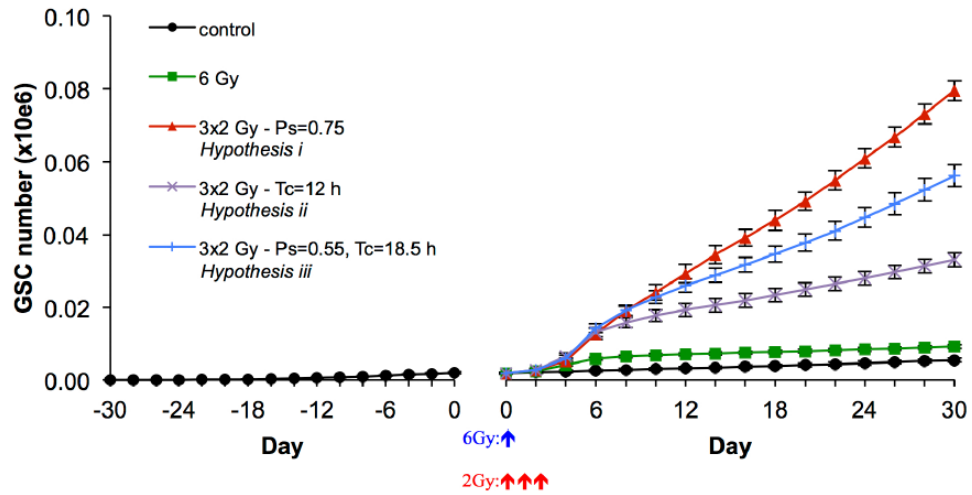


FIGURE 1.8: This figure [11] records the glioma stem cell numbers calculated by the CPM before and after treatment starts for all treatment cases including hypotheses. The error bars indicated the standard deviation in the data calculated by running the CPM 5 times.

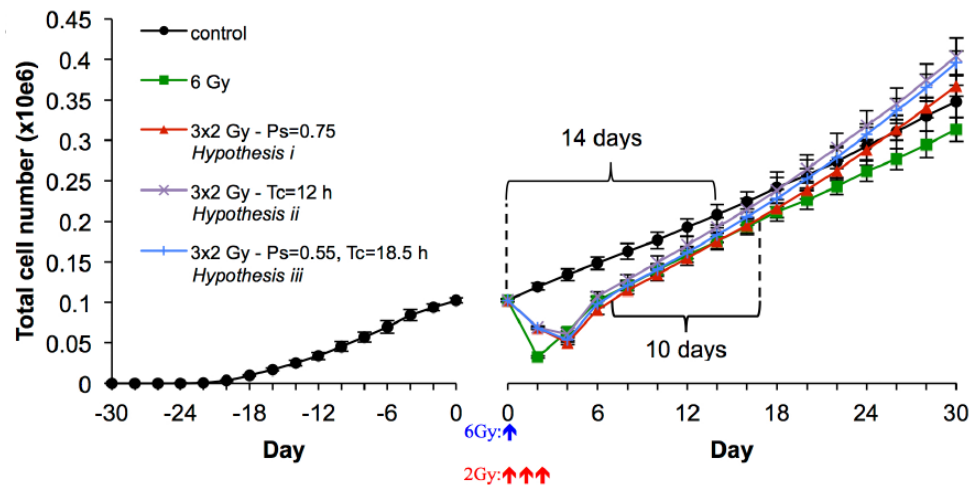


FIGURE 1.9: This figure [11] records the total cell numbers calculated by the CPM before and after treatment starts for all treatment cases including the hypotheses. The error bars indicated the standard deviation in the data calculated by running the CPM 5 times.

1.4.2 “*The tumour growth paradox and immune system-mediated selection for cancer stem cells*” T. Hillen, H. Enderling and P. Hahnfeldt.

In [14] Hillen *et al.* have constructed an integro-differential equation model that is simplified to an ordinary differential equation system. This ODE is used to model the *tumour growth paradox* using geometric singular perturbation theory. This model takes into account the interactions between cells within the tumour and basic cell properties that are often neglected.

Assumptions of this model

A mass of tumour contains a subpopulation of glioma stem cells and the remaining cells in the tumour population are classified as non-stem or cancer cells (CC). Similar to the assumptions in Gao’s paper, and subsequently in my thesis, the stem cells are assumed to be immortal with infinite proliferation capacity whereas the CC reproduce a finite number of times and die once their proliferation capacity is exhausted.

A GSC can divide into two daughter GSC or it can divide into a daughter GSC and a daughter CC. The authors refer to this cellular reproduction scenario as the *no symmetric commitment model*. The *no symmetric commitment model* is used to construct a mathematical model to simulate stem-cell-powered tumour growth.

A mathematical model of stem-cell-powered tumour growth

The tumour is made up of stem cells (GSC) and non-stem or cancer cells (CC). The number of cells per unit cell space (fraction of the interval $(x, x + dx)$ covered by cells) is defined as the cell density. $u(x, t)$ and $v(x, t)$ is the cell density at time t and location x for stem cells and cancer cells respectively. The authors define the total tumour density, $p(x, t)$, as follows:

$$p(x, t) = u(x, t) + v(x, t).$$

The maximum density per unit cell space is one cell only. Therefore, the total cell density is not greater than one ($p(x, t) \leq 1$). Cells can divide only if there is space for an

additional cell. A non-linear integral term $(\int_{\Omega} k(x, y, p(x, t))u(y, t)dy)$ is introduced to conduct spatial search for location for the daughter cells, where the kernel, $k(x, y, p(x, t))$ represents cell division occurring at location x from a mother cell at location y . If there is no space, cell division ceases. This is equivalent to the biological phenomenon of growth arrest.

Another assumption is that every ancestral cell at location y can give birth to only one daughter cell at location x in one cell cycle period. Therefore, $k(x, y, p(x, t)) \leq 1$. And $\int_{\Omega} k(x, y, p(x, t)) \leq 1$. This integral is the rate of cell division in one cell cycle over the domain from a parent cell at y . This integral cannot be greater than one as that implies that new particles, other than the daughter cells, are entering the system.

The frequency of cell cycles of the stem cells and the cancer cells are represented by γ and ρ respectively. Both these parameters are positive. The parameter δ is the probability of symmetric GSC divisions and α is the CC death rate. The system allows cell movement of GSC and CC through positive diffusion coefficients, D_u and D_v respectively. The domain of this system, $\Omega = R^n$, is smooth and bounded with either homogenous Neumann or Dirichlet boundary conditions.

Using the assumptions made above, the authors develop a system describing stem cell and cancer cell growth and interaction:

$$\begin{aligned} \frac{\partial u(x, t)}{\partial t} &= D_u \Delta u + \delta \gamma \int_{\Omega} k(x, y, p(x, t))u(y, t)dy, \\ \frac{\partial v(x, t)}{\partial t} &= D_v \Delta v + (1 - \delta) \gamma \int_{\Omega} k(x, y, p(x, t))u(y, t)dy \\ &\quad - \alpha v + \rho \int_{\Omega} k(x, y, p(x, t))v(y, t)dy. \end{aligned} \tag{1.1}$$

Homogenous Neumann boundary conditions can be used to model tumour growth in tissues where cells cannot permeate through bones or strong fibrous muscles. The homogenous Dirichlet boundary conditions can be used to model tumour growth where cells can leave blood vessels but are not allowed to return.

Reducing the system into ordinary differential equations

In order to simplify the integro-differential equation System 1.1, a few reductions and assumptions are made.

Reduction 1: Placement of a daughter cell only depends on the density, $p(x, t)$, of the final location of the daughter cell x , that is, $k = k(p(x, t))$. In addition to this reduction, the authors assume that the domain has unit volume. The mean densities of stem cells and cancer cells are

$$\bar{u}(t) = \int_{\Omega} u(y, t) dy, \quad \bar{v}(t) = \int_{\Omega} v(y, t) dy,$$

and so the mean density of the tumour population is $\bar{p}(t) = \bar{u}(t) + \bar{v}(t)$.

Reduction 2: Setting the density to be uniform across the domain, Ω . Along with this reduction, the authors assume uniform tumour growth across Ω . This implies that $k(p(x, t)) = k(\bar{p}(t))$, $u(x, t) = \bar{u}(t)$, $v(x, t) = \bar{v}(t)$ and $D_u = D_v = 0$.

These reductions simplify the integro-differential equations into the following ODE system:

$$\begin{aligned} \bar{u}_t(t) &= \delta \gamma k(\bar{p}(t)) \bar{u}(t), \\ \bar{v}_t(t) &= (1 - \delta) \gamma k(\bar{p}(t)) \bar{u}(t) - \alpha \bar{v}(t) + \rho k(\bar{p}(t)) \bar{v}(t). \end{aligned} \quad (1.2)$$

Assumption 1: $k(\bar{p}(t))$ is piecewise differentiable, $k(\bar{p}(t)) > 0$ for $0 \leq \bar{p}(t)$, $k(\bar{p}(t)) = 0$ for $\bar{p}(t) \geq 1$ and $k(\bar{p}(t))$ is decreasing for $0 \leq \bar{p}(t) < 1$. The authors choose $k(\xi) = \max\{1 - \xi^\sigma, 0\}$ where $\sigma \geq 1$.

Assumption 2: The GSC and CC growth rates, γ and ρ , are equal to 1.

System 1.2 is further simplified to:

$$\begin{aligned} \bar{u}_t(t) &= \delta k(\bar{p}(t)) \bar{u}(t), \\ \bar{v}_t(t) &= (1 - \delta) k(\bar{p}(t)) \bar{u}(t) - \alpha \bar{v}(t) + k(\bar{p}(t)) \bar{v}(t). \end{aligned} \quad (1.3)$$

Stability analysis of the ODE system

Adding the two equations above provides insight as to how the total tumour population density, $\bar{p}(t)$, changes over time, namely

$$\bar{p}_t(t) = k(\bar{p}(t))\bar{p}(t) - \alpha\bar{v}(t).$$

The growth rate of the total population of the cells, $\bar{p}_t(t)/\bar{p}(t) = k(\bar{p}(t)) - \alpha\bar{v}(t)/\bar{p}(t)$. This implies that CC slow down the overall tumour growth. Proliferation only occurs for $\bar{u}(t) + \bar{v}(t) \leq 1$. Therefore, the authors only perform stability analysis for the triangular, positively invariant region

$$\Delta = \{(\bar{u}(t), \bar{v}(t)) : 0 \leq \bar{u}(t) \leq 1, \bar{v}(t) \geq 0, \bar{u}(t) + \bar{v}(t) \leq 1\}.$$

This system of simplified ODEs has three steady states. These steady states are:

$$X_0 = (0, 0), X_V = (0, v_0), \text{ and } X_U = (1, 0).$$

By finding the Jacobian and analyzing the eigenvalues, the authors conclude that $X_0 = (0, 0)$ is a saddle for $\alpha > k(0)$ and an unstable node for $\alpha < k(0)$. The second fixed point, $X_v = (0, v_0)$, is a saddle for $\alpha < k(0)$. And the third fixed point, $X_u = (1, 0)$ is stable node or a stable spiral. In fact, X_u is the only attractor in the positively invariant region, Δ . Due to the absence of any equilibrium points in this region, the Poincare-Bendixon theorem says that $X_u = (1, 0)$ is globally asymptotically stable. This implies that for large time, the tumour will primarily consist of stem cells. However, the authors are mostly concerned about the short term dynamics of the system.

The authors varied α as a bifurcation parameter and discovered that the ratio $u(t)/v(t)$ over time varies for different values of α . For a small value of α , the tumour consists mainly of CC. However, for larger death rates, GSC thrive and, hence, the tumour size increases.

The tumour growth paradox

The authors provide a formal definition for this phenomenon:

Definition Let $P_\alpha(t)$ for times $t \geq 0$ denote a tumour population with a spontaneous death rate α for cancer cells. The population exhibits a tumour growth paradox if there exist death rates $\alpha_1 < \alpha_2$ and times t_1, t_2 and $T_0 > 0$ such that

$$P_{\alpha_1}(t_1) = P_{\alpha_2}(t_2) \text{ and } P_{\alpha_1}(t_1 + T) < P_{\alpha_2}(t_2 + T) \text{ for } (0 < T < T_0).$$

Hillen et al. [14] provided a proof of the *tumour growth paradox*. The following section contains a summary of the proof, employing geometric singular perturbation analysis.

Geometric singular perturbation analysis

In biological systems comprising of varied time scales, the geometric singular perturbation analysis is a helpful tool. This geometric approach uses invariant manifolds in phase space to understand the overall behaviour of the populations [13]. In the slow-fast system that the authors have studied is Equation (1.3), the parameter δ is a small parameter ($0 < \delta \ll 1$). With a change in time scale, $\tau = \delta t$, the System (1.3) can be rescaled to

$$\begin{aligned} \bar{u}_\tau(\tau) &= k(\bar{p}(\tau))\bar{u}(\tau), \\ \delta \bar{v}_\tau(\tau) &= (1 - \delta)k(\bar{p}(\tau))\bar{u}(\tau) - \alpha \bar{v}(\tau) + k(\bar{p}(\tau))\bar{v}(\tau). \end{aligned} \quad (1.4)$$

System 1.3 with a time scale represented by t , is the fast system, whereas System 1.4 with a time scale represented by τ , is the slow system. These systems are equivalent as long as $\delta \neq 0$. When the limit $\delta \rightarrow 0$ is applied, System (1.3) becomes

$$\begin{aligned} \bar{u}_t(t) &= 0, \\ \bar{v}_t(t) &= k(\bar{p}(t))\bar{u}(t) - \alpha \bar{v}(t) + k(\bar{p}(t))\bar{v}(t). \end{aligned} \quad (1.5)$$

The solutions to 1.5 are called the inner solutions. The slow manifold of the system is described by the fixed point of this system, $M = \{(\bar{u}_M, \bar{v}_M) : k(\bar{p}_M)\bar{p}_M - \alpha\bar{v}_M, \bar{p}_M = \bar{u}_M + \bar{v}_M\}$.

The long-scale dynamics of the system is given by the outer solution. Solutions for 1.4 quickly reach the slow manifold. To study the slow manifold in more detail, the authors provide a lemma:

Lemma *The slow manifold can be written as a graph $(\bar{u}, \bar{v}) = (\bar{u}, v_M(\bar{u}))$. Furthermore,*

$$\frac{d}{d\bar{u}}v_M(\bar{u}) = \frac{k'(\bar{p})\bar{p} + k(\bar{p})}{\alpha - k'(\bar{p})\bar{p} - k\bar{p}}, \text{ with } \bar{p} = \bar{u} + v_M(\bar{u}).$$

Given two death rates $\alpha_1 > \alpha_2$ then the slow manifold for α_1 is below the slow manifold of α_2 , i.e.,

$$v_M^{(1)}(\bar{u}) < v_M^{(2)}(\bar{u}).$$

The tumour growth paradox is a property of the slow manifold. A general result for the occurrence of the tumour growth paradox is outlined in the theorem below:

Theorem *Assume $\alpha_1 > \alpha_2 > 0$ and let $\bar{p}_1(t) = \bar{u}_1(t) + \bar{v}_1(t)$ and $\bar{p}_2(t) = \bar{u}_2(t) + \bar{v}_2(t)$ denote the corresponding solutions of the stem cell model. We assume that the tumour dynamics has settled onto the slow manifold M and that at time $t_0 \geq 0$, two tumours of equal size are presented $\bar{p}_1(t_0) = \bar{p}_2(t_0) = \bar{p}$, with $0 < \bar{p} < 1$. Then*

$$\frac{d}{dt}\bar{p}_1(t_0) > \frac{d}{dt}\bar{p}_2(t_0)$$

and

$$\bar{p}_1(t) > \bar{p}_2(t), \text{ for all } t > t_0.$$

The authors show that using Assumption 1, a large range of models display the property of the tumour growth paradox. This paradox is the accelerated growth of tumours as a result of increased cell death.

We will use the ODE model from this paper [14], namely (1.2). But instead of cell densities, $u(t)$ and $v(t)$ represent stem cell and cancer cell populations. We also use a

different kernel function. In our model, $k(p) = 1 - \frac{p}{C}$, where C is the carrying capacity. We will use this ODE model, adapt it to include treatment by irradiation and compare the findings with that of the CPM [11].

Chapter 2

Modelling glioma growth using Ordinary Differential Equations

The papers we have reviewed look at a simplified relationship between different types of cells in the GBM tumour. We will use the same assumptions to create our ODE model. The GBM consists of glioma stem cells (GSC), cancer cells (CC) and quiescent cells (QC). The glioma stem cells divide symmetrically with a probability of p_s (into daughter stem cells) or asymmetrically with a probability of $1 - p_s$ (into a daughter stem cell and a daughter cancer cell). This relationship is demonstrated in Figure 2.1. Glioma stem cells are known to have infinite proliferation capacity, which means that they are capable of reproducing forever, and they are immortal. However, cancer cells have finite proliferation capacity. This means that after reproducing a certain number of times, these cells die. The death rate of cancer cells is σ . A cell, stem or cancer, may become quiescent for a while to repair cellular injuries such as DNA damage. After recovering, these quiescent cells activate again into their former cell type.

2.1 A model with stem and non-stem cells

We will now develop a simple model that contains only stem and non-stem cells. Using the concepts we have learnt about symmetric and asymmetric division of stem cells (in Figure 2.1) and the assumptions made in the previous section, we construct a compartment figure. As shown in the compartmental diagram, Figure 2.2, the stem cells are

allowed to reproduce symmetrically with a probability of p_s or asymmetrically with a probability of $(1 - p_s)$. The growth rate of stem cells is k_G and the growth rate of cancer cells is k_C . The stem cells are immortal, therefore, they do not die. However, the cancer cells may die due to natural causes and the death rate for the cancer cells is σ .

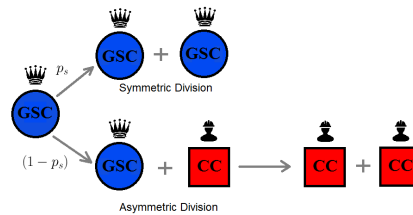


FIGURE 2.1: Symmetric and asymmetric division of glioma stem cells. The GSC divide symmetrically with a probability of p_s or asymmetrically with a probability of $1 - p_s$. CC on the other hand only divide symmetrically. The GSC (blue circles) are very powerful cells and are therefore represented by a crown, whereas the CC (red squares) are represented by a casual worker.

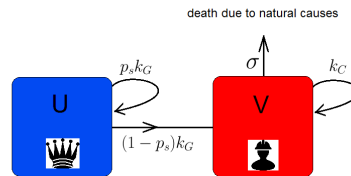


FIGURE 2.2: Model U,V: Glioma stem cells are denoted by U and non-stem (cancer) cells are denoted by V . There is no quiescent cell compartment in this model. GSC can divide into more GSC with a rate of $p_s k_G$ and can contribute to the CC compartment with a rate of $(1 - p_s) k_G$. The growth rate of CC is k_C and the death rate of CC is σ .

The corresponding ODE system (2.1) has volume constraint in all growth and division terms. Without this volume constraint, the ODE would be a linear system resulting in exponential growth of cells which is biologically unrealistic. The factor $(1 - \frac{U+V}{C})$ restricts the growth of cells to a carrying capacity of C .

$$\begin{aligned}
\dot{U} &= \overbrace{p_s k_G U \left(1 - \frac{U+V}{C}\right)}^{\text{symmetric division; growth}}, \\
\dot{V} &= \overbrace{(1-p_s)k_G U \left(1 - \frac{U+V}{C}\right)}^{\text{assymmetric division}} + \overbrace{k_C V \left(1 - \frac{U+V}{C}\right)}^{\text{growth}} - \overbrace{\sigma V}^{\text{natural death}}. \tag{2.1}
\end{aligned}$$

This ODE system resembles System 1.2 [14]. Our ODE system is a special case of Hillen et al.'s model [14]. We use a different kernel function, k , than that used in [14]. In our model, $k(p) = k(U+V) = 1 - \frac{U+V}{C}$, where C is the carrying capacity.

2.1.1 Fixed points and stability analysis

From (2.1), we see that $\dot{U} = 0$ when either $U = 0$ or $(1 - \frac{U+V}{C}) = 0$. Using these and setting $\dot{V} = 0$ we find the following fixed points:

$$(\bar{U}_1, \bar{V}_1) = (0, 0), (\bar{U}_2, \bar{V}_2) = (0, C(1 - \frac{\sigma}{k_C})), (\bar{U}_3, \bar{V}_3) = (C, 0). \tag{2.2}$$

In order for all these fixed points to be realistic, populations must be positive. Therefore,

$$k_C > \sigma, \tag{2.3}$$

otherwise, \bar{V} would be negative.

We now consider the stability of these fixed points. We start by finding the Jacobian matrix for this system,

$$J(\bar{U}, \bar{V}) = \begin{pmatrix} p_s k_G \left(1 - \frac{2\bar{U}+\bar{V}}{C}\right) & -p_s k_G \frac{\bar{U}}{C} \\ (1-p_s)k_G \left(1 - \frac{2\bar{U}+\bar{V}}{C}\right) - k_C \frac{\bar{V}}{C} & -(1-p_s)k_G \frac{\bar{U}}{C} + k_C \left(1 - \frac{\bar{U}+2\bar{V}}{C}\right) - \sigma \end{pmatrix}. \tag{2.4}$$

At the fixed point (\bar{U}_1, \bar{V}_1) , $J_{(0,0)} = \begin{pmatrix} p_s k_G & 0 \\ (1-p_s)k_G & k_C - \sigma \end{pmatrix}$.

The eigenvalues for the Jacobian at $(0, 0)$ are $\lambda_1 = p_s k_G > 0$ and $\lambda_2 = k_C - \sigma > 0$, using the condition stated in Equation (2.3). Therefore, the origin is an unstable fixed point.

At the fixed point $(\bar{U}_2, \bar{V}_2) = (0, C(1 - \frac{\sigma}{k_C}))$ the Jacobian is

$$J_{(0, C(1 - \frac{\sigma}{k_C}))} = \begin{pmatrix} p_s k_G \frac{\sigma}{k_C} & 0 \\ (1 - p_s) k_G \frac{\sigma}{k_C} - k_C(1 - \frac{\sigma}{k_C}) & k_C(-1 + \frac{2\sigma}{k_C}) - \sigma \end{pmatrix}.$$

The eigenvalues for the Jacobian at $(0, C(1 - \frac{\sigma}{k_C}))$ are $\lambda_1 = p_s k_G \frac{\sigma}{k_C} > 0$ and $\lambda_2 = k_C(-1 + \frac{2\sigma}{k_C}) - \sigma < 0$. Therefore, this fixed point is also unstable.

At the fixed point $(\bar{U}_3, \bar{V}_3) = (C, 0)$ the Jacobian is:

$$J_{(C, 0)} = \begin{pmatrix} -p_s k_G & -p_s k_G \\ -(1 - p_s) k_G & -(1 - p_s) k_G - \sigma \end{pmatrix}.$$

The trace of this Jacobian is $-p_s k_G - (1 - p_s) k_G - \sigma < 0$, the determinant of the Jacobian is $p_s k_G > 0$. Hence, $(C, 0)$ is a stable node or a stable spiral.

In order to determine the stability of these fixed points I performed a phase plane analysis. Refer to Figure 2.3, the triangular domain is a biologically significant region. We call this region biologically significant because firstly, cell populations ($U(t)$ and $V(t)$) cannot be negative. Secondly, when the total population is greater than the carrying capacity ($U(t) + V(t) > C$) the logistic function in Equation 2.1 is negative, therefore proliferation does not occur. So we will restrict our analysis to the region

$$\Delta = \{(U, V) : 0 \leq U \leq C, 0 \leq V \leq C, U + V \leq C\}.$$

Theorem 2.1. *For System 2.1, the region Δ is positively invariant.*

Proof. The boundaries of Δ are $U = 0$, $V = 0$ and $U + V = C$. Along the nullcline $U = 0$, the vector fields are as follows: $\dot{U} = 0$, $\dot{V} < 0$ for $V > C(1 - \frac{\sigma}{k_C})$ and $\dot{V} > 0$ for $V < C(1 - \frac{\sigma}{k_C})$. Along the second nullcline $U + V = C$, the vector field is $(0, -\sigma V)$ and points into the region Δ . Lastly, along the third line $V = 0$ that bounds Δ , the vector fields is described by $\dot{U} = p_s k_G U(1 - (\frac{U}{C})) > 0$ and $\dot{V} = (1 - p_s) k_G U(\frac{U}{C}) > 0$ for $U < C$. As shown in Figure 2.3, the vector fields along the boundary or into the region

Δ . Therefore, any solution trajectory that starts in Δ will stay within this region for $t \geq 0$. Hence, Δ is a positively invariant region. \square

Theorem 2.2. *The steady state $(C, 0)$ of the System 2.1 is globally asymptotically stable in the region Δ .*

Proof. The region Δ is positively invariant and $(C, 0)$ is the only stable equilibrium point in this invariant region. Therefore by the Poincare-Bendixon theorem, all solution trajectories tend to this equilibrium as $t \rightarrow \infty$. \square

We confirm this result by plotting the phase portrait on MATLAB using pplane7 (Figure 2.4) using biologically relevant parameters. These parameters are contained in a table in Chapter 7. In the phase portrait, we see that a slow manifold exists in the triangular invariant region that tends to the globally stable fixed point of $(C, 0)$. Biologically this means that as time goes to infinity, the entire tumour population (having a carrying capacity of C number of cells) will comprise of only stem cells. All other populations will die out. Even though we expect the tumour to consist purely of glioma stem cell population occurring at $t \rightarrow \infty$, we are concerned with what is happening at smaller time. The experimental data available to us only looks at stem cell composition of the GBM tumour over a few days. In addition to that, the survival period of the GBM tumour is approximately one year. This makes analyzing long time dynamics futile.

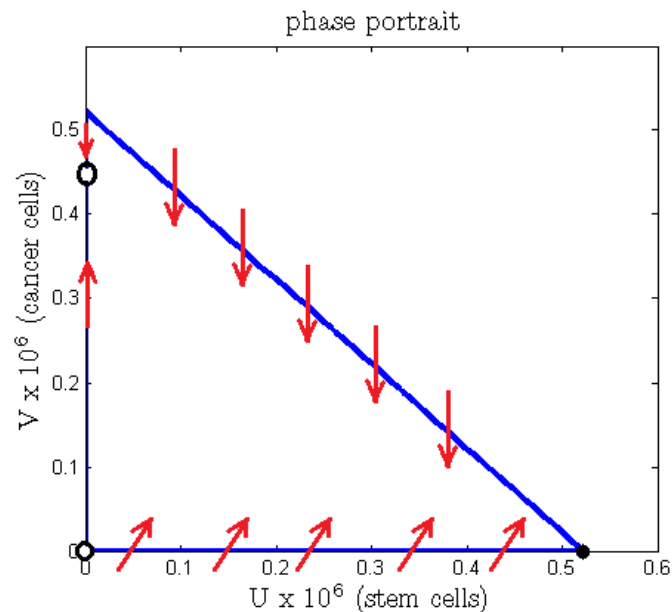


FIGURE 2.3: Phase portrait highlighting biologically significant invariant region (blue triangle), fixed points (black circles) and vector fields (red arrow)

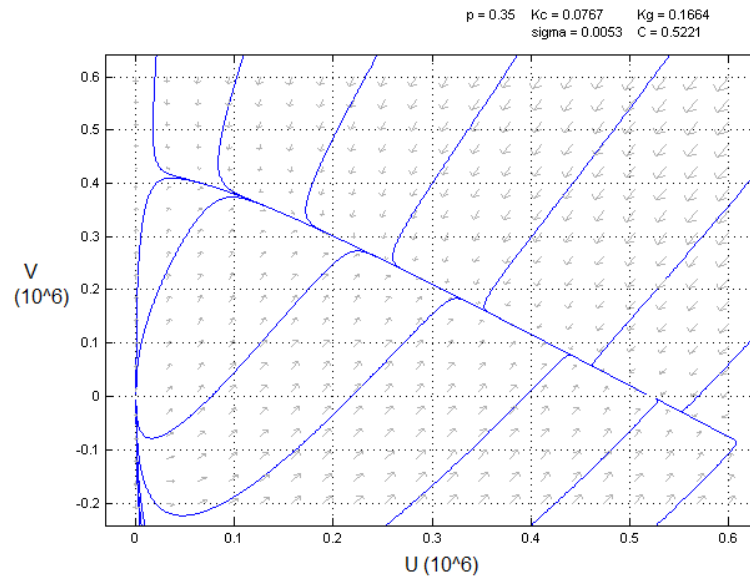


FIGURE 2.4: Phase portrait containing numerous numerical solution trajectories (blue lines), all of which are tending to the globally asymptotically stable steady state $(C,0)$. The direction of the vector fields are depicted by the black arrows.

2.2 Models with quiescence

After performing some mathematical analysis on the simple U, V model containing only stem cells and non-stem cells, we move on to create models that contain quiescence so that we can test those on the data which we have available. Quiescence is an important feature in biological systems. When cells suffer physiological or DNA damage due to changes in the environment, the cell's defence mechanism causes it to become growth arrested. As energy is not being utilized in increasing the cell's size or preparing it to divide, the cell can focus its energy on repairing DNA damage or producing proteins that help repair cell damage [5].

We have three models that contain quiescence. Model U, V, Qu allows stem cells to become quiescent with a rate of ν and return back into the stem cell compartment with a rate of μ . Similarly, model U, V, Qv allows cancer cells to become quiescent with a rate of ν and return back into the cancer cell compartment with a rate of μ . Lastly, the third model is the full model containing compartments U, V, Qu and Qv , where both the stem and the cancer cells are allowed to become growth arrested with a rate of ν_1 and ν_2 , respectively and return to their corresponding previous compartments with a rate of μ_1 and μ_2 , respectively.

These ODE systems with their corresponding compartment figures are shown below:

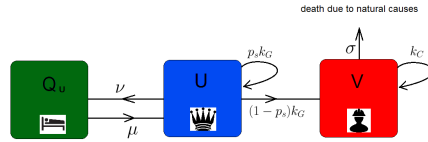


FIGURE 2.5: Model U,V,Q_U. This diagram is an extension of Figure 2.2. In addition to the assumptions of Model UV, the stem cells are allowed to become quiescent at a rate of ν and revert back at a rate of μ .

$$\begin{aligned}\dot{U} &= p_s k_G U \left(1 - \frac{U+V}{C}\right) + \mu Q_U - \nu U, \\ \dot{V} &= (1-p_s) k_G U \left(1 - \frac{U+V}{C}\right) + k_C V \left(1 - \frac{U+V}{C}\right) \\ &\quad - \sigma V, \\ \dot{Q}_U &= \nu U - \mu Q_U.\end{aligned}$$

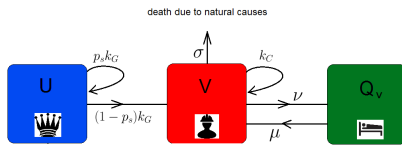


FIGURE 2.6: Model U,V,Q_V. This diagram is an extension of Figure 2.2. In addition to the assumptions of Model UV, the cancer cells are allowed to become quiescent at a rate of μ and revert back at a rate of ν .

$$\begin{aligned}\dot{U} &= p_s k_G U \left(1 - \frac{U+V}{C}\right), \\ \dot{V} &= (1-p_s) k_G U \left(1 - \frac{U+V}{C}\right) + k_C V \left(1 - \frac{U+V}{C}\right) \\ &\quad - \sigma V + \mu Q_V - \nu V, \\ \dot{Q}_V &= \nu V - \mu Q_V.\end{aligned}$$

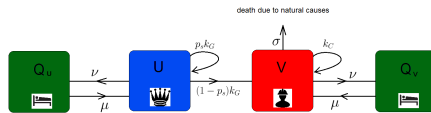


FIGURE 2.7: Model U,V,Q_U,Q_V: quiescence attributed to both stem cells (U) and cancer cells (V). U and V can become quiescent at a rate of ν_1 and ν_2 respectively and revert back at a rate of μ_1 and μ_2 respectively.

$$\begin{aligned}\dot{U} &= p_s k_G U \left(1 - \frac{U+V}{C}\right) + \mu_1 Q_U - \nu_1 U, \\ \dot{V} &= (1-p_s) k_G U \left(1 - \frac{U+V}{C}\right) + k_C V \left(1 - \frac{U+V}{C}\right) \\ &\quad - \sigma V + \mu_2 Q_V - \nu_2 V, \\ \dot{Q}_U &= \nu_1 U - \mu_1 Q_U, \\ \dot{Q}_V &= \nu_2 V - \mu_2 Q_V.\end{aligned}$$

Which of these models best predicts tumour growth? In the next chapter we will compare the UV , UVQ_U , UVQ_V and the UVQ_UQ_V models. We will use the least squares error method to fit the solutions of these models with tumour growth data from the Cellular Potts Model to find the most appropriate parameter set. Then we will compare these four models using the Akaike Information Criterion.

Chapter 3

Data fitting and model comparison

3.1 Estimating parameters to fit data

From the previous chapter, we now have four ODE models describing GBM tumour growth at our disposal. However, we are curious to find out which of these models best describes the tumour growth process. We will use statistical tests to compare these models amongst themselves and with glioma growth data. In order to compare these models, we will calculate the difference between the ODE solution and tumour growth data.

The glioma growth data is not experimentally determined. *In vitro* cell counting is done by a process called flow cytometry and requires glioma tissues growing in petri dishes to be broken down, thus collection of data containing cell numbers over a large period of time is difficult. Instead we use glioma growth data that was simulated by the CPM.

We contacted the authors of “*Acute and fractionated irradiation differentially modulate glioma stem cell division kinetics*” [11] at the Tufts University School of Medicine and obtained the data they had collected from the Cellular Potts Model. The Cellular Potts Model supplied 16 data points indicating the glioma stem cell numbers and the total cell numbers over a period of 30 days. We use this information to create a set of parameters that would make my ODE biologically realistic and comparable to the Cellular Potts

Model. In addition to that, once the data fit has been completed, the difference between the ODE solution and the *in silico* results from the CPM will be used to determine the best model using the Akaike Information Criterion (AIC).

3.1.1 The least-squares error method

In order to do parameter estimation, we used the least-squares error method [6]. The error calculated is the difference between the ODE solution of a GBM growth model and the matrix of cell numbers obtained from the CPM model. The solution to the ODE is denoted by $x = x(t_i; p, x_0)$, where p is the parameter vector, x_0 is the initial condition and the experimental data is denoted by y_i at time points t_i for $i = 1, \dots, n$. We received 16 data points depicting tumour growth over a time period of 30 days and so the number of data points is $N = 16$. Observed or experimental quantities are assumed to have stochastic effects. We assume that the error e_i is distributed normally with mean $\mu = 0$ and some variance σ^2 , $e_i \sim N(0, \sigma^2)$. Hence,

$$y_i = x(t_i; p, x_0) + e_i.$$

The likelihood for the ODE solution to be close to the experimental data is

$$\mathcal{L}(p) = \prod_{i=1}^n \frac{1}{\sqrt{2\pi}\sigma} e^{-\frac{y_i - x_i}{2\sigma^2}}.$$

However, calculating products is computationally more challenging than calculating sums. Consequently, we will work with the log of likelihoods:

$$\mathcal{LL}(p) = - \sum_{i=1}^n \ln(\sqrt{2\pi}\sigma) - \frac{1}{2\sigma^2} \sum_{i=1}^n (y_i - x_i)^2.$$

In order for the log-likelihood to be maximal for a parameter vector p , the residual sum of squares, or the error, must be minimized:

$$\begin{array}{l} \text{Residual Sum of Squares (error)} \\ \overbrace{D(p; x_0)} \end{array} = \sum_{i=1}^n \left(\overbrace{y_i}^{\text{Observed data (CPM)}} - \overbrace{x(t_i; p, x_0)}^{\text{Expected data (ODE)}} \right)^2.$$

We will now vary the parameters in our models over a biologically relevant range in order to find the values that best matches CPM results. The only parameter that is kept unchanged is p_s , the probability of symmetric division in glioma stem cells, as this value was determined experimentally [11].

Using the simplest model (UV: no quiescence) we vary the carrying capacity of our system, C , the growth rates of glioma stem cells and non-stem (or cancer) cells, k_G and k_C , respectively, and the death rate of non-stem cells, σ . Once we have a set of optimal values for these basic parameters, we move on to the more complicated quiescence models and vary the rate ν at which active cells become quiescent and the rate μ at which quiescent cells become active again.

3.1.2 Data fit using the optimal parameter set

Once we have obtained the optimal parameter set, we will use it to fit the corresponding models to the data. The data fit for the four models U, V , U, V, Q_u , U, V, Q_v and U, V, Q_u, Q_v are shown in Figures 3.1, 3.2, 3.3 and 3.4.

The first three models, UV, UVQu and UVQv seem to fit the data very closely. The fourth model, which is the full model UVQuQv does not look as effective. The formal comparison between models is conducted in the next section.

3.1.3 Improving the data fit

We notice that the initial stem cell number is approximately 2,000 stem cells and the initial total cell number is close to 100,000. As the magnitude of the total cell number is so high, while performing the least squares error method we are primarily fitting the ODE solution to the data representing the total cell number. In order to acknowledge the small stem cell population and have it contribute to the error, we should use the weighted least squares error method. In this method, the square of the difference between the stem cell data and the stem cell ODE solution is multiplied by a weight so that this error is of the same magnitude as the error calculated by the difference between the total cell data and total cell ODE solution. We will leave the exercise of implementing data fit using the weighted least squares error method as part of our future work.

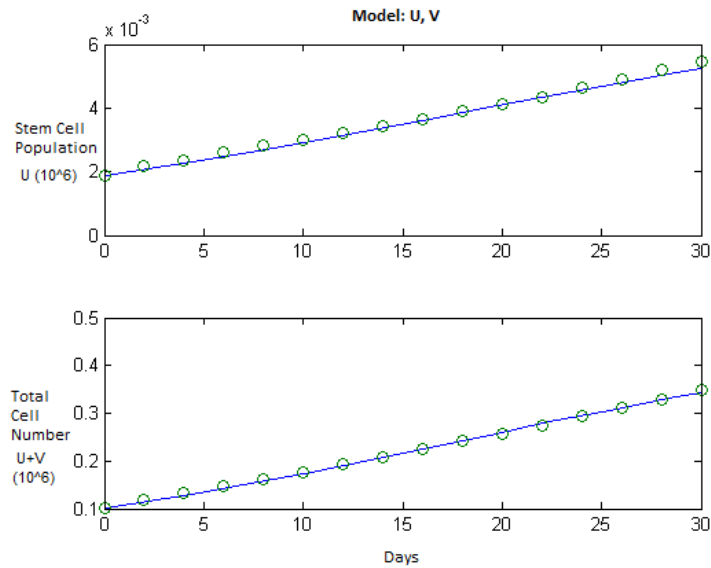


FIGURE 3.1: Data fitting for Model U,V: no quiescence. In the figure above, the green circles represent the CPM data and the blue line represents the ODE solution. The ODE model, containing stem (U) and non-stem (V), fits the CPM glioma growth data extremely well. The top graph is the number of stem cells ($U \times 10^6$) against time (in days), whereas the bottom graph is the total cell number ($(U+V) \times 10^6$) against time (in days).

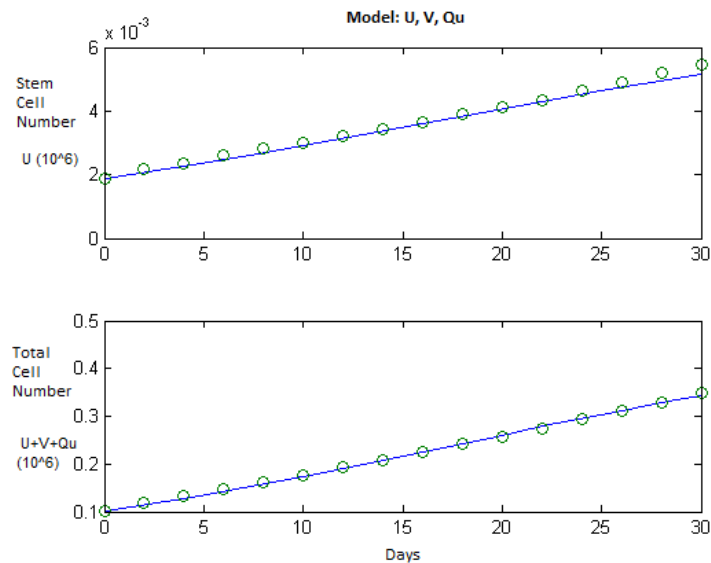


FIGURE 3.2: Data fitting for Model U,V,Qu: quiescence attributed to stem cells (U) only. In the figure above, the green circles represent the CPM data and the blue line represents the ODE solution. The ODE model, containing stem (U), cancer (V), and stem-derived-quiescent (Qu) cells, fits the CPM glioma growth data well. The top graph is the number of stem cells ($U \times 10^6$) against time (in days), whereas the bottom graph is the total cell number ($(U+V+Qu) \times 10^6$) against time (in days).

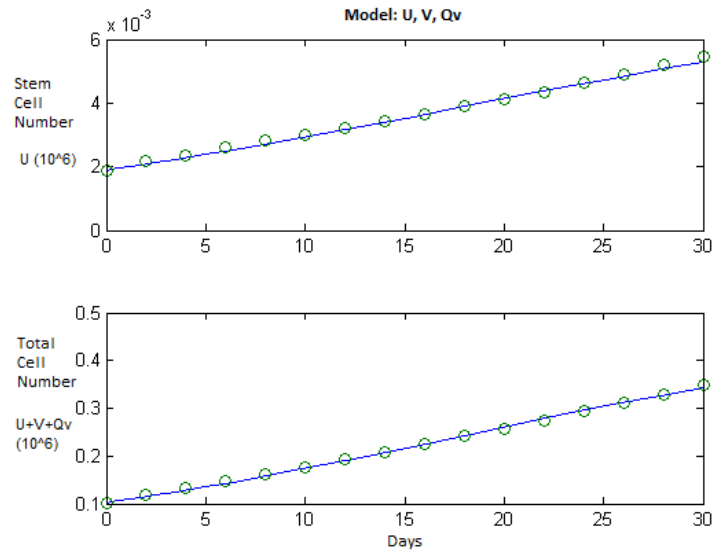


FIGURE 3.3: Data fitting for Model U, V, Q_v : quiescence attributed to cancer cells (V) only. In the figure above, the green circles represent the CPM data and the blue line represents the ODE solution. The ODE model, containing stem (U), cancer (V), and cancer-derived-quiescent (Q_v) cells, fits the CPM glioma growth data well. The top graph is the number of stem cells ($U \times 10^6$) against time (in days), whereas the bottom graph is the total cell number ($(U+V+Q_v) \times 10^6$) against time (in days).

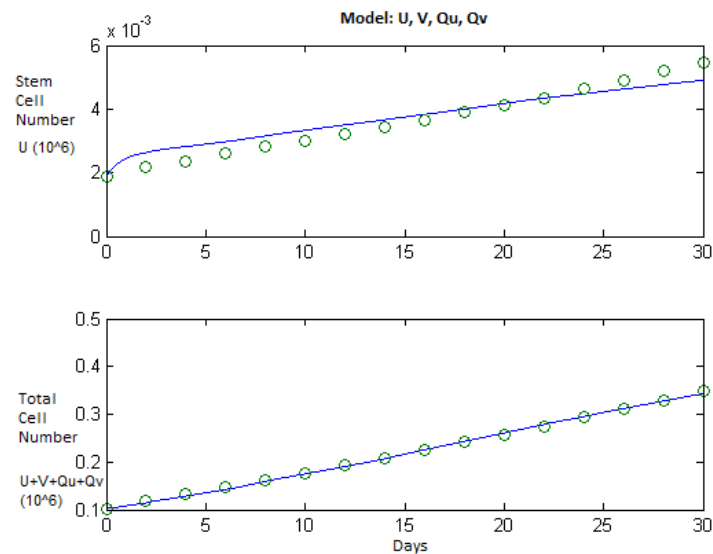


FIGURE 3.4: Data fitting for Model U, V, Q_u, Q_v : quiescence attributed to both stem cells (U) and cancer cells (V). In the figure above, the green circles represent the CPM data and the blue line represents the ODE solution. The ODE model, containing stem (U), cancer (V), stem and cancer-derived-quiescent (Q_u and Q_v) cells, does not fit the CPM glioma growth data well. The top graph is the number of stem cells ($U \times 10^6$) against time (in days), whereas the bottom graph is the total cell number ($(U+V+Q_u+Q_v) \times 10^6$) against time (in days). Resultant bad fit is due to the absence of information on how quiescent cell populations behave in the glioma growth CPM model.

3.2 Model comparison using the Akaike Information Criterion

Suppose we have two models to explain a given set of data. If both of these models have the same number of parameters, n_p , then comparing the likelihoods or the log-likelihoods is enough to compare these models. The model with the higher likelihood is better suited to describe the process. How then do we compare models that have a different number of parameters? The Akaike Information Criterion (AIC) is used to compare models that contain a different number of parameters [6]. It is defined as follows:

$$AIC = \underbrace{2\mathcal{L}\mathcal{L}(\hat{p})}_{\text{maximum log-likelihood}} - 2 \underbrace{n_p}_{\text{number of parameters}}.$$

The larger the AIC, the better the model. However, if the number of data points, N , is small ($N \leq 40$), then the following *corrected AIC* should be used [6]:

$$AIC_c = 2\mathcal{L}\mathcal{L}(\hat{p}) - 2n_p \frac{N}{N - n_p - 1}.$$

As our analysis uses only 16 data points ($N = 16$), we will use the corrected AIC to compare the four ODE models.

We used the ODE solutions and the tumour growth data to find the residual sum of squares (or the error), the variance, the log-likelihoods, and the corrected AIC for all four models. The results are shown in Table 3.1.

model	U, V	U, V, Q_u	U, V, Q_v	U, V, Q_u, Q_v
n_p	5	7	7	9
Error (D)	1.889(10^{-4})	2.0213(10^{-4})	1.9974(10^{-4})	1.4792(10^{-4})
$\sigma^2 = \frac{D}{N=16}$	1.1806(10^{-5})	1.2633(10^{-5})	1.2359(10^{-5})	9.2452(10^{-6})
$\mathcal{L}\mathcal{L}(p)$	68.0722	67.5303	67.7060	70.0282
AIC_c	120.1444	107.0610	107.4119	92.0564

TABLE 3.1: Comparing models. This table contains the number of parameters, n_p , error, D , variance, σ^2 , log-likelihoods, $\mathcal{L}\mathcal{L}(p)$, and the corrected AIC for the four ODE models (UV, UVQu, UVQv, UVQuQv) that we wish to compare. As the AIC_c of model UV is the highest, it is the best model amongst the four.

3.3 Conclusion

The model containing no quiescence, that is the UV model, has the highest AIC and is therefore the best model for our data.

This makes sense because the data available to us only gives the number of stem cells and the total number of cells. There is no information about the behaviour of the quiescent cell population, nor do we know how to differentiate between the cancer cells and the quiescent cells. Thus predicting the rates ν and μ from the limited data is difficult. We will base our future analysis on model U, V .

Chapter 4

Mathematics of the derivation of radiation treatment: The Linear-Quadratic Model

In the previous chapters, we constructed ODE systems that modelled tumour growth and we chose the best amongst them. In this chapter, we will add the aspect of treatment of tumours to the model. The linear quadratic model is used to incorporate irradiation treatment into mathematical and individual-based models. In the Cellular Potts Model [11], the number of cells that survived treatment was calculated by the survival ratio based upon the linear-quadratic model. In the next section, we will discuss the survival ratio in more detail and will construct a function which represents the linear quadratic model that we can use in our differential equation model.

4.1 The Linear-Quadratic Model

Cell death occurs in a tumour in response to radiotherapy. The linear-quadratic model (LQ) is an apt choice to model cell killing due to ionizing radiation. The linear-quadratic model describes the effect of radiation on tissues and was developed by considering the bio-physical events that occur in the cellular nucleus when a tissue undergoes radiotherapy.

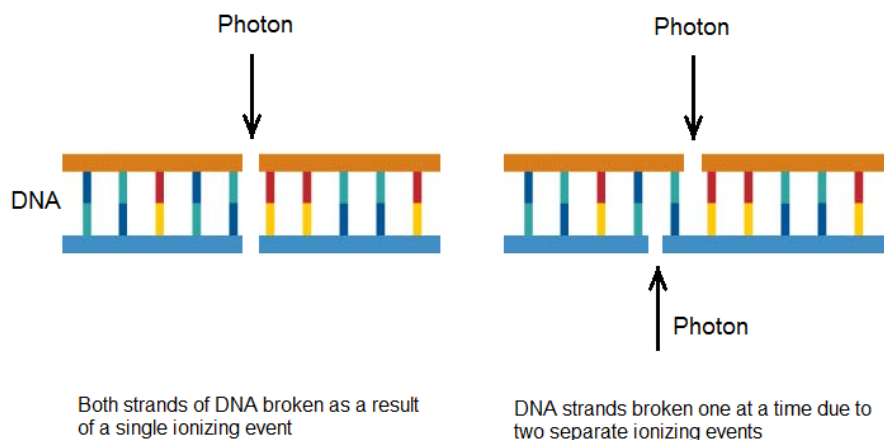


FIGURE 4.1: Two cases discussing how lethal damage to a cell happens when a double strand break occurs in the DNA caused by gamma-ray photons.

The linear-quadratic model assumes that cell death due to radiation can occur either as a result of a single ionizing event or as a result of two separate ionizing events. In the former case, a cell undergoes a DNA double strand break due to a single photon. In the latter case, the cell undergoes a double strand break in the DNA due to two separate radiation tracks (in other words, two separate photons, each photon damaging one DNA strand). This is summarized in Figure 4.1. If the time between the photon attacks is large, the single strand break may be repaired, in which case there is no lethal damage [3]. Also, in order for cell death to happen, the two single strand breaks should occur within a few base pairs of each other.

The linear-quadratic model predicts that the yield of lethal DNA damage is proportional to $\alpha D + \beta D^2$, where D is the radiation dose and parameters α and β are radio-sensitivity coefficients [12]. The probabilistic measure of DNA's double strand break occurring due to a single photon is α (of units Gy^{-1}), whereas β (of units Gy^{-2}) is the probabilistic measure of DNA's double strand break occurring due to two separate photons [4].

The parameters α and β are rarely known, individually. However, the $\frac{\alpha}{\beta}$ ratio is known and provides insight as to how effective different kinds of radiation treatments will be on a tissue. In other words, this ratio is a quantitative measure of the sensitivity of a tissue to variation in dose fractionation [4]. The ratio $\frac{\alpha}{\beta}$ is the dose (in units of Gy) at which the two types of DNA damage (damage due to single photon and separate, double photons) are equal. At doses smaller than $\frac{\alpha}{\beta}$ Gy, cell death occurs primarily due

to DNA damage by a single photon, whereas at doses greater than $\frac{\alpha}{\beta}$, cell death occurs due to two separate ionizing events.

The $\frac{\alpha}{\beta}$ value for tumours (5-25 Gy) is higher than normal tissues values (2-5 Gy) [4]. The glioblastoma multiforme tumour has a very high $\frac{\alpha}{\beta}$ value. The GBM tumours are usually treated by external beam radiotherapy. In this form of radiotherapy, radiation is administered from a source outside the patient's body. Treatments where high doses have to be administered are usually broken down into fractions so that the healthy tissue can repair between treatments. In order to calculate the ratio of cells in a tumour that survive after irradiation treatment, the survival ratio is used:

$$S(D) = e^{-\lambda(\alpha D + \beta D^2)}, \quad (4.1)$$

where D is the ionizing radiation dose, the parameter λ describes the radio-protection of different cells found in a single tissue and λ_U, λ_V and λ_Q are the radio-protection parameters for stem cells, cancer cells and quiescent cells, respectively. When a total treatment of dose D is broken up into n fractions of smaller dose d , the linear-quadratic survival ratio is modified as the cell survival for each dose is independent [12]. The LQ survival ratio for fractionated treatment is:

$$S(D) = e^{-\lambda(\alpha + \beta d)D}, \quad (4.2)$$

where $D = nd$.

The linear-quadratic model is the most commonly used mechanism to predict the effects of radiotherapy. This is because it requires few parameters and is derived by biological reasoning. The LQ model has been tested clinically and it has been said to predict cell death successfully in tissues that have received radiotherapy for up to 10 Gy units per fraction of total dose [2].

The Cellular Potts Model used the parameter values given in Table 4.1 to calculate the GBM tumour's response to radiotherapy [11]. In the numerical analysis for the ODE models, the experimentally determined values mentioned in Table 4.1 will be used.

Parameter	Meaning	Value
α	radio-sensitivity parameter for single-hit cell death	0.3859 Gy^{-1}
β	radio-sensitivity parameter for single-hit cell death	0.01148 Gy^{-2}
λ_U	radio-resistance parameter for glioma stem cells	0.1376
λ_V	radio-resistance parameter for cancer cells	1
λ_Q	radio-resistance parameter for quiescence cells	0.5

TABLE 4.1: This table contains experimentally determined values of the radio-sensitivity coefficients (α and β) and the radio-protection coefficients (λ_U , λ_V and λ_Q) of the cells present in the GBM tumour. These values were used in the CPM [11] and have also been used in the current project.

4.2 Hazard Function

In order to incorporate the linear-quadratic survival ratio into the ODE system, we use the hazard function. The hazard function, $h_{LQ}(t)$, is described as the decay rate of the survival ratio [12]:

$$\frac{dS(D(t))}{dt} = -h_{LQ}(t)S(D(t)). \quad (4.3)$$

Equation (4.3) can be obtained using Equation (4.1), the initial conditions $t = 0$, $D(0) = 0$, and $S(D(0)) = S(0) = 1$, and a hazard function (4.4) (This function was first proposed by Zaider and Minerbo [12]) such as

$$h_{LQ}(t) = \lambda(\alpha + 2\beta D(t))\dot{D}(t). \quad (4.4)$$

The derivation of Equation (4.3) from (4.4) is shown below:

$$S(D(t)) = e^{-\lambda(\alpha D(t) + \beta D(t)^2)}$$

$$\ln S(D(t)) = -\lambda(\alpha D(t) + \beta D(t)^2)$$

$$\ln S(D(t)) - \ln 1 = -[(\lambda(\alpha D(t) + \beta D(t)^2)) - \lambda(\alpha D(0) + \beta D(0)^2)]$$

$$\ln S(D(t)) - \ln S(D(0)) = -\lambda(\alpha D(t) + \beta D(t)^2)|_0^t$$

$$\int_{S(0)}^{S(D)} \frac{1}{q} dq = - \int_0^t \lambda(\alpha + 2\beta D(p)) dD(p)$$

$$\int_{S(0)}^{S(D)} \frac{1}{q} dq = - \int_0^t \lambda(\alpha + 2\beta D(p)) \frac{dD(p)}{dp} dp$$

let: $h_{LQ}(t) = \lambda(\alpha + 2\beta D(t))\dot{D}(t)$ [12]

$$\int_{S(0)}^{S(D(t))} \frac{1}{q} dq = - \int_0^t h_{LQ}(p) dp$$

$$\frac{1}{S(D(t))} dS(D(t)) = -h_{LQ} dt$$

$$\frac{dS(D(t))}{dt} = -h_{LQ}(t)S(D(t))$$

Case 1: If the treatment includes a single dose, d , of ionizing radiation, then $D(t) = d$. This preserves the linear quadratic model as the survival ratio remains the same. That is, $S(D(t)) = S(d) = e^{\lambda(-\alpha d - \beta d^2)}$.

Case 2: If a fractionated dose is administered, which means that the treatment consists of n fractions of dose d , then by the end of the treatment, the survival ratio looks like $S(D(t)) = e^{\lambda(-\alpha nd - \beta (nd)^2)}$. In this case, the term containing β is exaggerated due to the presence of n^2 . This is not in line with the linear-quadratic model and so a different hazard function for fractionated treatment is proposed [12]. This hazard function is

$$h_{LQ}^f(t) = (\alpha + \beta d)\dot{D}(t).$$

Using the same derivation technique used above and $h_{LQ}^f(t)$, we can derive the LQ survival ratio for fractionated treatments (Equation 4.2).

Figures 4.2 and 4.3 demonstrate what the hazard functions looks like for two different kinds of treatment. Figure 4.2 describes the ionizing radiation treatment that occurs at

day zero and is of 6 Gy units. The treatment depicted in Figure 4.3 is of 2 Gy units of ionizing radiation conducted at day zero, one and two. We approximate each fraction by a smooth Gaussian concentrated at the corresponding treatment time. In all future analysis, we will be using the treatments depicted in Figures 4.2 and 4.3, namely the single ionizing radiation (IR) treatment and the fractionated IR treatment, respectively.

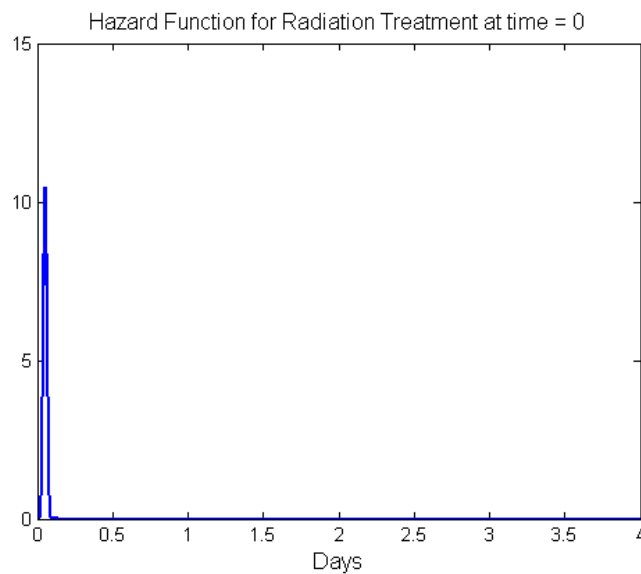


FIGURE 4.2: The hazard function for a single ionizing radiation treatment of 6 Gy administered on day 0.

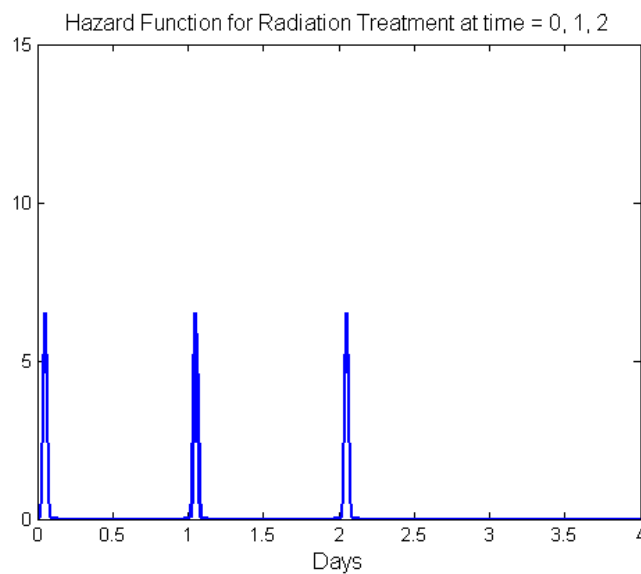


FIGURE 4.3: The hazard function for fractionated ionizing radiation treatment of 2 Gy administered on three consecutive days (Day 0, 1, and 2)

Chapter 5

Glioma stem cell model with radiation treatment

We created several systems containing glioma stem cells and non-stem cells to model tumour growth in Chapter 2. In Chapter 3, we went on to test these models and concluded that the model containing no quiescence best predicted the data. In Chapter 4, we discussed how the linear-quadratic survival ratio of cells, after they have been exposed to ionizing irradiation, can be adapted to ordinary differential equations using a hazard function. We will now bring the findings of the last three chapters together. By including a “death by irradiation term”, that is accounted for by the hazard function, we are modifying our glioma growth model (Equations 2.1) into a glioma treatment model (Equations 5.1) . The treatment model is as follows:

$$\begin{aligned}\dot{U} &= p_s k_G U \left(1 - \frac{U+V}{C}\right) - h_{LQ_U}(t)U, \\ \dot{V} &= (1 - p_s)k_G U \left(1 - \frac{U+V}{C}\right) + k_C V \left(1 - \frac{U+V}{C}\right) - \sigma V - h_{LQ_V}(t)V. \quad (5.1)\end{aligned}$$

For treatments comprised of a single dose $D = d$, the hazard function is $h_{LQ}^s(t)$. For treatments where the dose D is administered in multiple (n) fractions of smaller dose (d), that is $D = nd$, the hazard function is $h_{LQ}^f(t)$ (refer to Equation set 5.2).

$$h_{LQ_i}^s(t) = \lambda_i(\alpha + 2\beta D(t))\dot{D}(t), \quad (5.2)$$

$$h_{LQ_i}^f(t) = \lambda_i(\alpha + \beta d)\dot{D}(t), \quad (5.3)$$

where $i = U, V$. As the stem cells (U) and cancer cells (V) have different tolerance to radiotherapy, we require the hazard function to take that into account. Therefore, the radio-protection coefficient, λ_i , in the hazard function varies for the two types of cells. The hazard functions for the stem cells and cancer cells are given by h_{LQ_u} and h_{LQ_v} respectively. The parameters α and β are radio-sensitivity parameters for single and double hit cell killing respectively.

5.1 ODE results and comparison with experimental data

The ODE system (Equations 5.1) is solved numerically using the *ode45* function in Matlab. The ODE solution is plotted from the time of the treatment (day zero) to 48 hours after the last treatment (as shown in Figure 5.1).

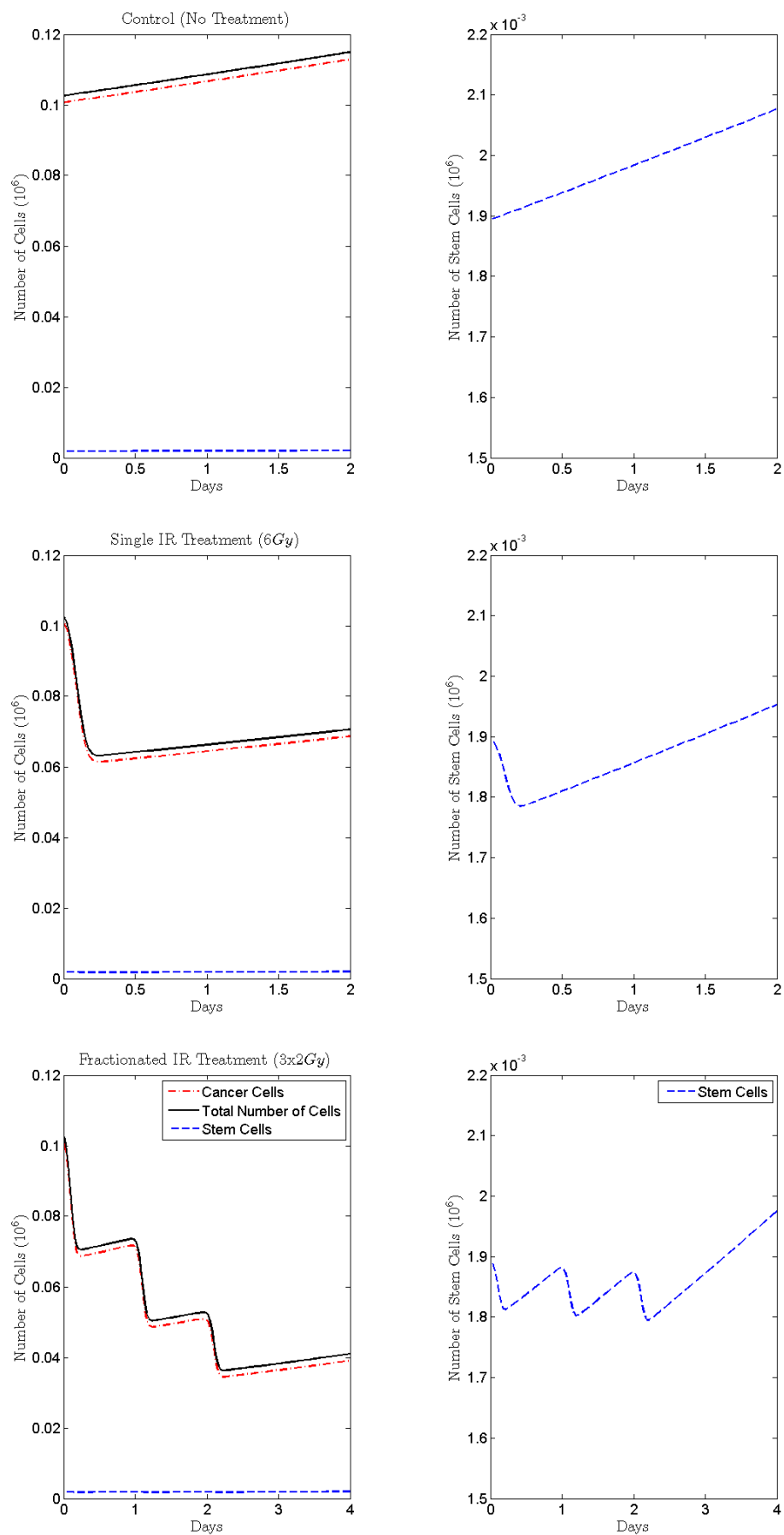


FIGURE 5.1: ODE solutions for growth of tumour that received no treatment (control case), for tumour that received treatment by single irradiation dose at $t = 0$ and for tumour that received treatment by fractionated irradiation dose at times $t = 0, 1, 2$.

In order to validate our results, we will compare outputs obtained by the ODE model with *in vitro* results. I have chosen to compare my results with the data obtained by experiments on the U87 glioma cell line [16]. The stem cell percentage is calculated 2 days after the last treatment and is compared to experimentally determined glioma stem cell percentages shown in Figure 1.6 [16].

The bar graph in Figure 5.2 compares glioma stem cell fraction obtained experimentally to that obtained by our ODE model. In the control case, both the *in vitro* and ODE glioma stem cell percentages are close to $\approx 1.8\%$. This is because in Chapter 3, we determined a set of parameters that minimized the least-squares error of the difference between the ODE solution and the CPM results of stem cell numbers. As a result, the no-treatment case's stem cell percentage is very close to the experimental results.

However for the treatment cases (both, single and fractionated treatments), the ODE system underestimates the stem cell percentage. The predicted percentage of glioma stem cells in a tumour that has been treated using a single dose of 6 Gy of ionizing radiation is $\approx 2.8\%$ and those treated using a fractionated dose of 2 Gy administered on three consecutive days have a GSC% of $\approx 4.8\%$. Experimentally however, the glioma stem cells make up a larger fraction of the tumour. Despite the underestimation, the trend observed *in vitro* seems to be conserved by the ODE system. The percentages obtained from the ODE predict an increase in the glioma stem cell ratios as treatment type varies from single to fractionated dose. In addition, the glioma stem cell percentage for fractionated treatment in both, *in vitro* and ODE simulations, are almost twice that of the stem cell percentages for the single treatment case.

We observe a discrepancy between the percentage of glioma stem cells predicted by our ODE system and the data provided by the lab. Even though the trend is conserved, there is a $\approx 47 - 54\%$ difference between ODE results and *in vitro* data. Is there a biological change occurring due to irradiation that causes glioma stem cell percentage to increase after the tumour is exposed to irradiation in the lab? As it turns out, there is!

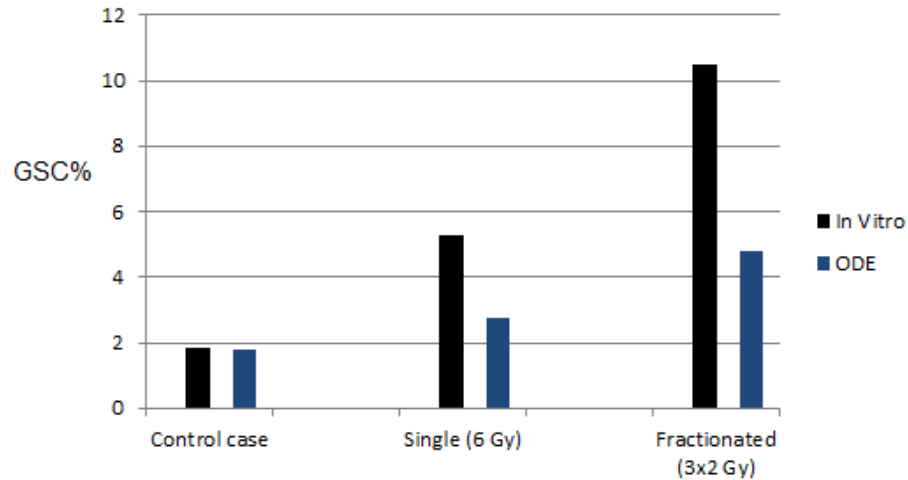


FIGURE 5.2: This figure compares the GSC% calculated from the ODE solution to those determined experimentally 48 hours after the last irradiation dose. The black bars are the U87 glioma stem cell percentages from Figure 1.6. The blue bars are the GSC percentages calculated from the ODE solutions.

5.2 Cell behaviour changes after irradiation treatment

Ionizing radiation affects several glioma stem cell signalling pathways. SHh, Notch, Wnt, EGFR and AKT/cyclin D1/Cdk4 are amongst the pathways that are most affected [1]. When a tumour is exposed to γ -radiation, the Notch2 and the Wnt pathways are up-regulated in the glioma stem cell [24]. This results in a higher probability of symmetric division. In other words, glioma stem cells divide symmetrically into two glioma stem cells more often than dividing asymmetrically into a stem cell and a cancer cell. In addition to the Notch and Wnt pathways, ionizing radiation activates the AKT/ cyclin D1/Cdk4 pathway in human glioma stem cells which results in a shorter G1 phase [21]. Hence, a shorter cell cycle results. A shorter cell cycle implies that the glioma stem cells are growing faster, or that the growth rate of these stem cells has increased.

These biological findings imply that there are changes that need to be made in our ODE model. We can do this by allowing the parameters that control the type of division and growth rate of the glioma stem cells to vary. The two parameters we will now vary are p_s , the probability of symmetric division and k_G , the growth rate of glioma stem cells.

In the next chapter, we will perform sensitivity analysis for these parameters to see how they impact the ODE system's outcome.

Chapter 6

Sensitivity analysis

In the previous chapter, we discussed how irradiation can affect the chemistry of a glioma stem cell resulting in a faster growth rate and a higher chance of symmetric division. We can account for these changes in our ODE model by varying the parameters p_s , the probability of symmetric division in glioma stem cells and k_G , the growth rate of glioma stem cells. We will now perform sensitivity analysis to see how these two parameters impact the output from the ODE model.

Sensitivity analysis is a technique used to determine how the model responds to perturbation of an input. Or in other words, it is an investigation of how different values of a parameter will impact a particular dependent variable. To calculate the sensitivity, $S_p(y)$, of a dependent variable, $y(p)$, we use the following formula (Equation 6.1). The variable, $y(p)$, depends on a parameter, p , and p^* is the reference value of p :

$$S_p(y) = \frac{\partial y}{\partial p} \frac{p^*}{y(p^*)}. \quad (6.1)$$

For our model, the dependent variable is G , the glioma stem cell percentage. And the parameters that affect G are p_s , the probability of symmetric division, and k_G , the growth rate of glioma stem cells. Using (6.1) to calculate sensitivity, we deduce the sensitivity of G on p_s and k_G for different treatments using reference points $p_s = 0.35$ and $k_G = 0.167$ (these values are from the optimal parameter set for the control case and were determined using the least squares error method in Chapter 3). The sensitivities are computed as follows:

- For treatment using a single dose of 6 Gy:

- $S_{p_s}(G) = 0.159$,

- $S_{k_G}(G) = 0.299$.

What this implies is that, in the ODE model of single dose treatment, for a 1% increase in the probability of symmetric division, p_s , the glioma stem cell percentage, G , calculated 2 days after the last treatment, increases by 0.159%. And for a 1% increase in the growth rate of glioma stem cells, k_G , the glioma stem cell percentage, G , increases by 0.299%. This means that G is more sensitive to changes in k_G than p_s . This is also depicted in Figure 6.1, as the slope of the curve of G due to changes in k_G is steeper than the slope of the curve of G as p_s varies.

- For treatment using a fractionated dose of 2 Gy administered on three consecutive days:

- $S_{p_s}(G) = 0.323$,

- $S_{k_G}(G) = 0.546$.

In the fractionated dose treatment, for a 1% increase in the probability of symmetric division, p_s , in the ODE model, the glioma stem cell percentage, G , calculated 2 days after the last treatment, increases by 0.323%. And for a 1% increase in the growth rate of glioma stem cells, k_G , the glioma stem cell percentage, G , increases by 0.546%. Just as was observed in the single treatment case, this means that G is more sensitive to changes in k_G than p_s . This is also depicted in Figure 6.2 as the slope of the curve of G due to changes in k_G is steeper than the slope of the curve of G as p_s varies.

We can therefore conclude that in both cases, variation in k_G impacts the glioma stem cell percentage more than variation in p_s .

Also, Figure 6.1 indicates that simply varying either the growth rate of glioma stem cells or the probability of symmetric division, in the ODE model, will not get us a result that corresponds with the experimental data. In fact, both k_G and p_s need to be increased in order to obtain a stem cell percentage that is close to the *in vitro* data. In the fractionated case, we notice that a high enough increase in k_G in the ODE model, predicts the stem cell percentage to be the same as experimental data. But in order to

have a universal explanation that explains both, the single and fractionated treatment results, we will hypothesize that not one but both parameters, p_s and k_G , are altered when a tumour undergoes ionizing radiation treatment.

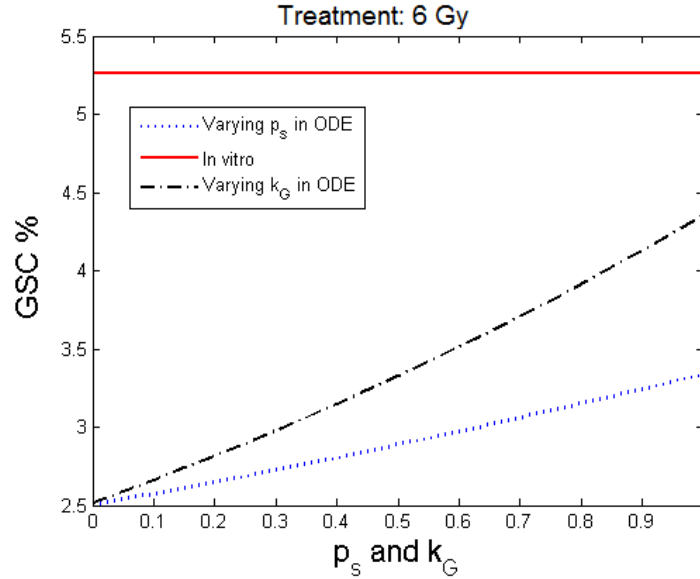


FIGURE 6.1: Parameters p_s and k_G are varied in the ODE model for tumours treated with a single irradiation dose and GSC% is compared with that found in *in vitro* experiments. The graph demonstrates that GSC% is more sensitive to the parameter k_G than p_s . In tumours treated with a single irradiation dose, variation in either p_s or k_G is not enough to explain the enrichment of GSC % in *in vitro* tumours. Hence, an increase in both p_s and k_G must occur in order to accommodate this change.

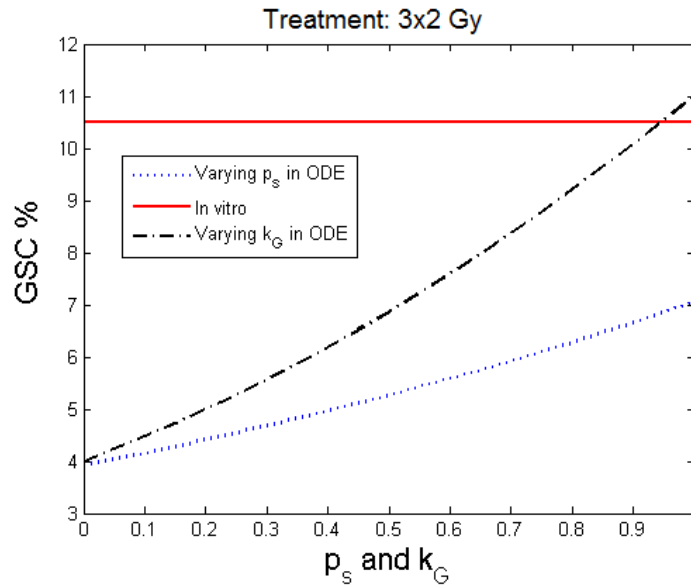


FIGURE 6.2: Parameters p_s and k_G are varied in the ODE model for tumours treated with fractionated irradiation dose and GSC% is compared with that found in *in vitro* experiments. The graph demonstrates that GSC% is more sensitive to the parameter k_G than p_s . In tumours treated with multiple irradiation doses, increase in k_G is enough to explain the enrichment of GSC % in *in vitro* tumours. However, only increasing p_s does not predict the GSC % enrichment observed *in vitro*.

6.1 Main results

We varied the values of p_s over the interval $(0, 1)$ and k_G over a realistic range. The stem cell percentage for these values were calculated using our glioma treatment ODE model. The difference between the stem cell percentage calculated from the single treatment ODE and that observed *in vitro* was calculated and squared. The same was done for the fractionated treatment. These differences were then added, this made up the total error. Errors were calculated for all values of p_s and k_G . The values for p_s and k_G for which the error was minimum were selected. In this way, we obtained the best possible fraction of glioma stem cells when compared to experimental result. The outcome is shown in Figure 6.3. The optimal values are $p_s = 0.55$ and $k_G = 0.56$. When compared to the parameter values from the control case, there is a $\approx 57\%$ increase in the probability of symmetric division and a $\approx 229\%$ increase in the glioma stem cell growth rate once ionizing radiation therapy is applied to the tumour. With these new parameter values, the glioma stem cell percentage 48 hours after the last dose is better predicted. In the single dose radiation treatment case, the modified ODE predicts that the GSC percentage will be 4.16% (experimentally, this percentage was 5.26%). In the fractionated dose radiation treatment, the modified ODE predicts that the GSC percentage will be 10.59% (experimentally, this percentage was 10.5%). These are better results than that of the unmodified ODE.

A possible improvement to our model would be to set the parameters p_s and k_G as functions of the irradiation treatment. That is, these parameters would be functions of the dose $D(t)$. Therefore, when the radiotherapy dose is non-zero, the values of p_s and k_G will increase depending on the number of fractions the dose is split into. Incorporating $p_s(D(t))$ and $k_G(D(t))$ in our glioma treatment model is left as an exercise for future work.

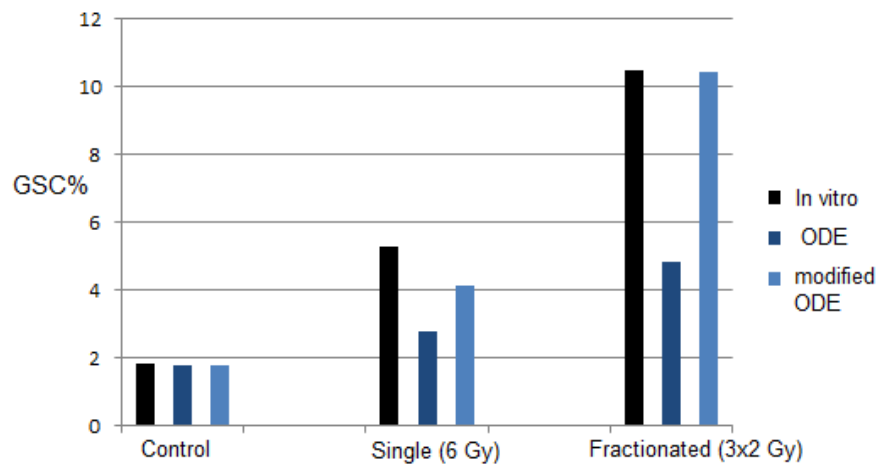


FIGURE 6.3: GSC% calculated 2 days after the last irradiation dose. The black bars represent the GSC% determined experimentally using the U87 glioma cell line (illustrated in Figure 1.6 [16]). The dark blue bar represent the GSC% calculated from the solution of the unmodified ODE. The light blue bars represent the GSC% calculated from the solution of the ODE that was modified after sensitivity analysis was performed on parameters p_s and k_G .

Chapter 7

Discussion

7.1 Future work: Adding quiescence to our model using a delay

One of the biological properties of tumours that undergo irradiation treatment is the property of growth arrest. Growth arrest occurs when a cell is distressed and needs to take some resting time in order to recover from damage. When a tumour is irradiated, DNA damage occurs. To recover from that, glioma stem cells go into quiescence mode. This phase lasts for approximately 16 hours [11]. As we are comparing outcomes from the differential equations to that of the Cellular Potts Model, we want all the assumptions made in the Cellular Potts Model to be reflected in our differential equation model also.

The Cellular Potts Model accounts for growth arrest of cells as a consequence of irradiation treatment. Our ODE model, on the other hand, does not. In Chapter 3, we considered models where quiescent cells existed in addition to stem and cancer cells. But a comparison of the models by the Akaike Information Criterion we concluded that the quiescence models did not fit the tumour growth data as nicely as the no-quiescence model did. Hence, the models containing quiescence were rejected.

In Chapter 6, we compared the results from the Cellular Potts Model to that of our ODE. But can we compare two models that do not have the same assumptions? We will now try to incorporate growth arrest into our differential equation system in order to obtain a system that has the same assumptions as the Cellular Potts Model.

We construct a delay differential equation system that incorporates growth arrest, caused by radiation treatment, into our ODE model. In layman terms, this delay differential equation system says that from all the glioma stem cells that were eradicated by treatment, some of these cells return with a rate of γ_U after a delay of $\tau = 16$ hours. Similarly, amongst all the cancer cells that were removed due to treatment, some return with a rate of γ_V after a delay of $\tau = 16$ hours. However, as the glioma stem cells are greatly resistant to radiation and the cancer cells are far less resilient, we keep $\gamma_V \ll \gamma_U$. The corresponding delay model reads:

$$\begin{aligned}\dot{U} &= p_s k_G U \left(1 - \frac{(U+V)}{C}\right) - h_{LQ_U}(t)U + \gamma_U h_{LQ_U}(t-\tau)U(t-\tau), \\ \dot{V} &= (1-p_s)k_G U \left(1 - \frac{(U+V)}{C}\right) + k_C V \left(1 - \frac{(U+V)}{C}\right) - \sigma V \\ &\quad - h_{LQ_V}(t)V + \gamma_V h_{LQ_V}(t-\tau)V(t-\tau).\end{aligned}\tag{7.1}$$

For variable recovery time, that is when the delay τ is not fixed, the recovery rate of growth-arrested stem cells is $\gamma_U = \theta_U e^{-\eta_U \tau}$, where θ_U is the rate of transition of a quiescent stem cell to become an active stem cell again and the term $e^{-\eta_U \tau}$ is the proportion of cells that survive treatment. Similarly, $\gamma_V = \theta_V e^{-\eta_V \tau}$ is the recovery rate of growth-arrested cancer cells.

Does incorporating growth arrest into our differential equation actually make a difference? The Cellular Potts Model's results that we have seen so far are outcomes of a system that allows growth arrest after treatment. However, for fractionated treatment, the Cellular Potts Model also considered a case where the cells do not go into arrest. We will use that result to observe how a model containing quiescence compares to a model that does not consider quiescence. We notice that in both, the Cellular Potts Model and the differential equation model, the glioma stem cell percentage is lower in models that contain quiescence to those models who did not consider quiescence. This is shown in the bar graphs in Figure 7.1

As part of our future work, we will do sensitivity analysis on the DDE model. Consider Figure 7.2. In this figure, we compare the GSC percentages predicted by the unmodified ODE and DDE with the *in vitro* GSC percentages. The results from the DDE are

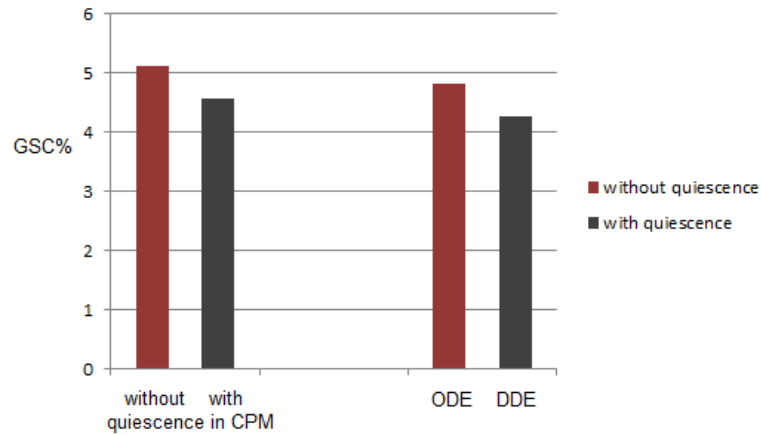


FIGURE 7.1: This bar graph compares GSC % calculated using both CPM and differential equation models, in cases where quiescence (using delay) is considered and when quiescence is not considered. The red bars represent the model that does not account for quiescence in the system. Whereas, the grey bars represent models that incorporate the assumption of quiescence.

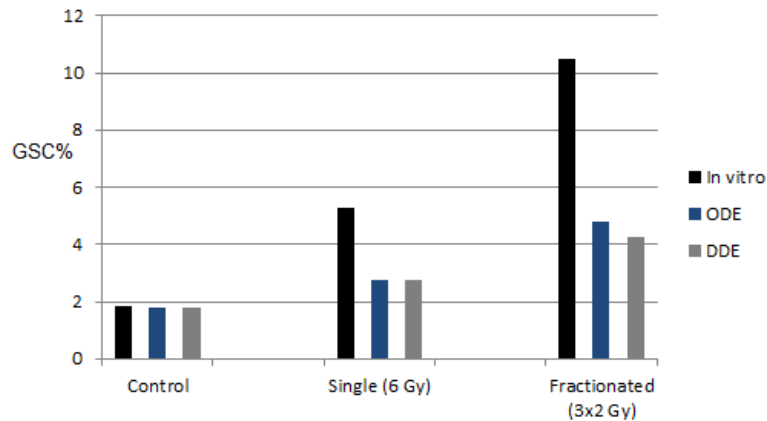


FIGURE 7.2: GSC% calculated 2 days after last irradiation dose. The black bars represent GSC% determined in vitro, the blue bars represent GSC% calculated from the ODE model and the grey bars represent GSC% calculated using the DDE model.

similar to ODE results. Sensitivity analysis using the parameters p_s and k_G may give us a similar observation as that made in the modified ODE model.

7.2 Discussion and Conclusions

The Glioblastoma Multiforme (GBM) is a heterogenous mass of tumour cells. These tumour cells have different characteristics. We have created a mathematical model that uses ordinary differential equations to predict population dynamics of these cells. Our model uses the following assumptions: The stem cells (known throughout this thesis as

glioma stem cells (GSC)) are powerful cells that are capable of dividing continuously without dying. Whereas, the non-stem cells (referred to as cancer cells (CC)) are mortal cells that divide till their proliferation capacity runs out. We conduct analysis on our model and conclude that as time tends to infinity, the tumour will comprise only of stem cells.

We include treatment to this mathematical model using the linear-quadratic concept of cell death due to radiotherapy. Different types of treatment, including treatment administered in a single dose and treatment administered in multiple smaller doses are compared. We analyze how different treatments may affect the tumour composition of cells. As the glioma stem cells are resistant to radiation (an assumption that was considered in our ODE model), an increase in the stem cell ratio in the tumour was expected after treatment. Our mathematical model results confirmed this. However, the *in vitro* data demonstrated that the GSC percentages in the GBM after irradiation were a lot higher than that predicted by the ODE model. Gao et al. [11] claimed that there is a radiation-induced biological alteration occurring in the glioma stem cell that causes enrichment in their population.

Gao et al. hypothesized that after radiotherapy that has been administered in fractionated doses, the glioma stem cell dynamics change. The likelihood of a glioma stem cell to undergo symmetric division is higher. The chances of symmetric division to occur may increase from as low as 35% to as high as 75% (literature suggests that these conditions are possible [11]). In addition to that, the glioma stem cell has a significantly shorter cell cycle of 12 hours instead of the normal length of 25 hours. The authors also include the case where both radiation-induced events occur, that is, the chances of symmetric division increase partially and the cell cycle shortens to 18.5 hours. If the CPM takes these changes into account, the fraction of glioma stem cells in the simulated GBM tumour is comparable to *in vitro* data. The authors conclude that even though the CPM predicts a suitable glioma stem cell percentage two days after the last irradiation dose for all three cases, increase in the rate of symmetric division seems to be the dominant reason as to why there is radiation-induced enrichment of GSC in the tumour.

Using our ODE model, we set out to test Gao et al.'s hypotheses. We do not only consider the case where the tumour is irradiated with fractionated doses but also the case where the tumour receives a single dose of ionizing radiation. We perform sensitivity

analysis using the parameters that influence the glioma stem cell cycle's length and the cell's ability to divide symmetrically, namely k_G and p_s respectively.

Our major finding was that contrary to the conclusion derived from a CPM-simulated GBM, the dominant mechanism for the increment in GSC fraction in the ODE-simulated GBM is the shorter cell cycle induced by radiotherapy. In other words, in any kind of radiotherapy treatment, single-dosed or fractionated, the GSC percentage is more sensitive to the growth rate of stem cells. In fact, the increase in the probability of symmetric division alone is not enough to explain the enrichment of GSC ratios in the GBM tumour. Another important finding of our ODE model was that as the treatment dose is broken up into more fractions, the model becomes increasingly sensitive to variation in parameters p_s and k_G . In addition to that, these parameters increase GSC percentage in the ODE model for fractionated treatment more than in the ODE model for single dose treatment.

In conclusion, similar to the Cellular Potts Model, our ODE model indicates that the radio-resistant feature of glioma stem cells is not enough to explain the abnormal enrichment of stem cell ratios after radiotherapy *in vitro*. This increase in the stem cell fractions is instead a result of radiation-induced increased stem cell population. The increase in stem cell population, after treatment, is attributed to faster cell cycle and a shift in symmetric division of glioma stem cells.

Parameters	C	p_s	k_G	k_C	σ	α	β	λ_U	λ_V	γ_U	τ
Control	0.5221	0.35	0.1664	0.0767	0.0053						
Determined by	Least-squares	Gao et al. [11]	Least-squares	Least-squares	Least-squares						
IR treatment						0.3859	0.01148	0.1356	1	1.5	0.667
Determined by	The	same	values	were	used	[11]	[11]	[11]	[11]		

TABLE 7.1: This table records the parameter values used throughout this project. This table also mentions the source where these parameters were derived from.

Bibliography

- [1] **Beachy, P. A., Karhadkar, S. S., Berman, D. M.** (2004) *Tissue repair and stem cell renewal in carcinogenesis*. Nature, 432(7015),324-31.
- [2] **Brenner, D. J.** (2008) *Point: the linear-quadratic model is an appropriate methodology for determining iso-effective doses at large doses per fraction*. Semin. Radiat. Oncol., 18(4),234-239
- [3] **Dale, R. G.** (1985) *The application of the linear quadratic dose-effect equation to fractionated and protracted radiotherapy*. Brit. J. Radiol., 58(690),515-528.
- [4] **Dale, R.** (2004) *Use of the linear-quadratic radiobiological model for quantifying kidney response in targeted radiotherapy*. Cancer Biotherapy and Radiopharmaceuticals, 19(3),363-370.
- [5] **Dawson, A., Hillen, T.** (2006) *Derivation of the tumor control probability (TCP) from a cell cycle model*. Computational and Mathematical Methods in Medicine, 7(2-3),121-141.
- [6] **DeVries, G., Hillen, T., Lewis, M., Muller, J., Schonfisch, B.** *A course in mathematical biology: Quantitative modelling with mathematical and computational methods*. (2006) SIAM
- [7] **Dingli, D., Michor, F.** (2006) *Successful therapy must eradicate cancer stem cells*. Stem Cells, 24(12), 2603-2610.
- [8] **Enderling, H., Hlatky, L., Hahnfeldt, P.** (2009) *Migration rules: tumours are conglomerates of self-metastases*. Br. J. Cancer, 100(12), 1917-1925.
- [9] **Enderling, H., Anderson, A. R. A., Chaplain, M. A. J., Beheshti, A., Hlatky, L., Hahnfeldt, P.** (2009) *Paradoxical dependencies of tumor dormancy and progression on basic cell kinetics*. Cancer Res., 69(22), 8814-8821.

- [10] **Ganguli, R., Puri, I. K.** (2006) *Mathematical model for the cancer stem cell hypothesis*. Cell Prolif., 39, 3-14.
- [11] **Gao, X., McDonald, J. T., Hlatky, L., Enderling, H.** (2013) *Acute and fractionated irradiation differentially modulate glioma stem cell division kinetics*. Cancer Research. 73(5)1481-90.
- [12] **Gong, J., Dos Santos, M. M., Finlay, C., Hillen, T.** (2011) *Are more complicated tumor control probability models better?* Mathematical Medicine and Biology, 30(1),1-19.
- [13] **Hek, G.** *Geometric singular perturbation theory in biological practice*. (2010) Journal of Mathematical Biology. 60(3), 347-386.
- [14] **Hillen, T., Enderling, H., Hahnfeldt, P.** (2013) *The tumor growth paradox and immune system-mediated selection for cancer stem cells*. Bulletin of Mathematical Biology, 75(1),161-84.
- [15] **Holland, E. C.** (2006) *Glioblastoma multiforme: the terminator*. Proceedings of the National Academy of Sciences, 97(12),6242-6244.
- [16] **Kim, M. J., Kim, R. K., Yoon, C. H.** (2011) *Importance of PKC δ signalling in fractionated-radiation-induced expansion of glioma-initiating cells and resistance to cancer treatment*. Journal of Cell Science, 124(18)3084-3094.
- [17] **Nduom, E. K., Hadjipanayis, C. G., Meir, C. G.** (2012) *Glioblastoma cancer stem-like cells: Implications for pathogenesis and treatment*. The Cancer Journal, 18(1),100-106.
- [18] **Omuro, A., DeAngelis, L. M.** (2013) *Glioblastoma and other malignant gliomas: a clinical review*. Journal of the American Medical Association, 310(17),1842-1850.
- [19] **Powathil, G. G., Adomson, D. J. A., Chaplain, M. A. J.** (2013) *Towards predicting the response of a solid tumour to chemotherapy and radiotherapy treatments: clinical insights from a computational model*. PLOS Computational Biology, 9(7), 1-14.
- [20] **Ramirez, Y. P., Weatherbee, J. L., Wheelhouse, R. T., Ross, A. H.** (2013) *Glioblastoma multiforme therapy and mechanisms of resistance*. Pharmaceuticals, 6,1475-1506.

-
- [21] Shimura, T., Noma, N., Oikawa, T., Ochiai, Y., Kakuda, S., Kuwahara, Y. et al. (2012) *Activation of AKT/cyclin D1/Cdk4 survival signalling pathway in radioresistant cancer stem cells*. Nat. Rev. Cancer, 1(6):e12.
- [22] Sole, R. V., Rodriguez-Caso, C., Diesboeck, T. S., Saldance, J. (2008) *Cancer stem cells as the engine of unstable tumor progression*. Journal of Theoretical Biology, 253(4), 629-637.
- [23] Swat, M. H., Belmonte, J., Heiland, R. W., Zaitlen, B. L., Glazier, J. A., Shirinfard, A. *Introduction to CompuCell3D: Version 3.6.2*. Biocomplexity Institute and Department of Physics, Indiana University.
- [24] Ulasov, I., Nandi, S. (2011) *Inhibition of Sonic Hedgehog and Notch pathways enhances sensitivity of CD133+ Glioma stem cells to temozolomide therapy*. Mol. Med. The Feinstein Institute for Medical Research, 17(1-2):1
- [25] Vescovi, A. L., Galli, R., Reynolds, B. A. (2006) *Brain tumour stem cells*. Nature Reviews Cancer. 6, 425-436.
- [26] Xie, Q., Mittal, S., Berens, M. E. (2014) *Targeting adaptive glioblastoma: an overview of proliferation and invasion*. Neuro-Oncology, 0,1-10.
- [27] Zhang, X., Zhang, W., Mao, X. G., Zhen, H. N., Cao, W. D., Hu, S. J. (2013) *Targeting role of glioma stem cells for glioblastoma multiforme*. Curr. Med. Chem. 20(15),1974-84.